Article:
Abdalla, T. and Peng, C. (2025) Spatiotemporal variability of PM2.5 infiltrations in higher education buildings: a multizone air-thermal co-simulation analysis. Journal of Building Engineering, 111. 113473. ISSN: 2352-7102

https://doi.org/10.1016/j.jobe.2025.113473

Spatiotemporal variability of PM2.5 infiltrations in higher education buildings: A multizone air-thermal co-simulation analysis

Article reference	JOBE_113473
Journal	Journal of Building Engineering
Corresponding author	Chengzhi Peng
First author	Tha'er Abdalla
Received at Editorial Office	28 Mar 2025
Article revised	17 Jun 2025
Article accepted for publication	14 Jul 2025

DOI: 10.1016/j.jobe.2025.113473

Spatiotemporal variability of $PM_{2.5}$ infiltrations in higher education buildings: A multizone air-thermal co-simulation analysis

Abstract

Exposure to outdoor-sourced particulate matter with an aerodynamic diameter of 2.5 micrometres or less ($PM_{2.5}$) infiltration poses significant health risks to occupants of Higher Education Institution (HEI) buildings. Unlike residential settings, HEI buildings are complex and heterogeneous, presenting unique challenges for comprehensive Indoor Air Quality (IAQ) assessment. This study addresses this gap by employing a novel high-resolution multizone air-thermal co-simulation approach to investigate $PM_{2.5}$ infiltration dynamics across 2,729 zones from an HEI building stock, which is crucial when consistent long-term monitoring data is unavailable. Hourly time series data reveal significant spatial and temporal variations in indoor $PM_{2.5}$ concentrations and air change rates (ACH_{INF}), underscoring the necessity of room-level resolution for accurate assessment in HEI environments. Our results demonstrate a clear positive impact of improving building airtightness (Q_{50}) on indoor $PM_{2.5}$ levels. For instance, reducing Q_{50} from 13 $m^3/h/m^2$ (leaky) to 3 $m^3/h/m^2$ (well-sealed) significantly decreased zones exceeding the WHO 2005 guideline (10 $\mu g/m^3$) from 82% to merely 1%. Crucially, the study also revealed that outdoor $PM_{2.5}$ background concentrations in the study location already frequently exceeded WHO 2005 annual guidelines (e.g., an average of 17.04 $\mu g/m^3$ during the heating season). Consequently, even with well-sealed buildings (Q_{50}=3 $m^3/h/m^2$), a significant proportion (approaching 88%) of zones still exceeded the more stringent WHO 2021 guideline of 5 $\mu g/m^3$. These findings underscore the critical interplay between building airtightness and ambient pollution levels in determining indoor air quality and highlight the limit of what airtightness alone can achieve in highly polluted outdoor environments.

Keywords: $PM_{2.5}$ infiltrations, building airtightness, higher education institution (HEI) buildings, multizone air-thermal co-simulation, spatiotemporal variability of indoor $PM_{2.5}$

1. Introduction

Particulate matter with an aerodynamic diameter of 2.5 micrometres or less ($PM_{2.5}$) air pollution is a major threat to health worldwide. It is described as one of the "great killers of our age" because of its varied and severe effects on human health (Venkatesan, 2016). Several studies have shown that excessive exposure to high $PM_{2.5}$ concentrations reduce the expected lifespan of humans by one to five years (Apte et al., 2018; Cserbik et al., 2020). In 2013, the World Health Organization (WHO) identified particulate matter as the leading cause of human cancer (WHO, 2013). Research over the past 15 years has shown that even low levels of $PM_{2.5}$ can cause significant health risks, including cardiovascular and respiratory diseases, lung cancer, and premature death (Feng et al., 2016; Chen et al., 2023). Updated in September 2021, the latest WHO Air Quality Guideline sets the recommended annual $PM_{2.5}$ limit at 5 $\mu g/m^3$, a reduction from the 2005 guideline of 10 $\mu g/m^3$, and the 24-hour average $PM_{2.5}$ level was adjusted from 25 $\mu g/m^3$ to 15 $\mu g/m^3$ (WHO, 2021). The update reflects the new scientific evidence and growing understanding of the severe health impacts of air pollution and the need for stronger action to reduce exposure.

Since HEI building users often spend long hours indoors, there is a concern about chronic exposure to indoor air pollutants such as fine particulate matter ($PM_{2.5}$) in particular. Daily running of HEI premises involves a substantial number of building users and facilities, making potential environmental degradation caused by intensive energy use. There is a common concern that energy

consumption in HEI buildings should be effectively managed to reduce waste and environmental impacts. Hence, most HEIs have implemented energy management strategies and programs to align campus operations with sustainability goals. In the UK, an example is the University of Sheffield Energy Strategy developed to achieve net-zero carbon emissions by 2030 (Arup, 2012). HEI energy strategies often include information on the current energy use patterns and provide information on where building interventions, such as fabric upgrades and increasing the airtightness of building envelopes, are planned and scheduled. A critical challenge lies in balancing energy efficiency and IAQ, as efforts to enhance building airtightness for energy conservation can adversely affect IAQ by increasing exposure to indoor air pollutants.

Both direct and indirect methods have been developed and applied to assess IAQ in single buildings or across entire building stocks. Direct methods include field measurements using mobile or stationary air quality (AQ) sensors of varying grades. However, obtaining direct field measurements of $PM_{2.5}$ at a large-scale with high-grade AQ monitoring can be prohibitively expensive and time-consuming. Also, direct methods seldom capture the complex dynamic interactions of air particles and transient behaviours within a building or a group of buildings. This is due to the limitations imposed by either the instrumental factors (e.g. device selection, calibration and reliability) or the sampling methods (e.g., measurement location, sampling frequency and time-averaging period) (Coleman & Meggers, 2018; Jones et al., 2018). Moreover, there can be uncertainties associated with individual or a network of IAQ sensors, resulting in measurements that may be potentially misleading (O'Leary et al., 2019).

Indirect methods primarily involve computational modelling, simulation, and statistical techniques, which may offer several advantages over direct measurements in certain situations, such as cost-effectiveness, flexibility in assessing different scenarios and interventions, and time efficiency. Nevertheless, it is essential to acknowledge that simulation models rely on abstractions and assumptions, and their robustness and accuracy depend on both the quality of the input data and the expertise of the modellers. Below we first review the state of the art in building simulation for IAQ assessment.

2. Rationale, novelty, and consideration of broader applicability

This study was motivated by an overarching concern that energy policies in the current UK HEI context, which often promote building airtightness as an intervention to reduce energy consumption, may inadvertently neglect its impact on IAQ (ECA, 2003; Klepeis et al., 2001; Schweizer et al., 2007); that building envelopes with enhanced airtightness may raise building users' exposure to indoor air pollution (Smith et al., 2016; Vardoulakis, 2009). Higher education institution (HEI) buildings are a distinct and under-studied building type for several reasons: (1) HEI buildings are often located in high-density urban built areas, and air pollution from urban traffic and other sources is the most significant contributor to substandard indoor air quality (IAQ) (Afroz et al., 2023); (2) HEI buildings differ from typical office or residential buildings in their size, spatial complexity, and diversity of uses (e.g., classrooms, laboratories, offices, libraries, circulation spaces). This leads to highly variable airflow patterns and pollutant distributions, necessitating high-resolution, multi-zone modelling approaches; and (3) The unique occupancy schedules and high density of users in HEI buildings result in distinct exposure profiles compared to other building types.

While previous research has examined indoor air quality (IAQ) in various building types, our study makes several novel contributions to the field. **First**, we apply a coupled CONTAM-EnergyPlus simulation framework to model the spatiotemporal variability of $PM_{2.5}$ infiltration across 2,729

zones in a representative HEI building stock. This level of spatial and temporal detail is not seen in the literature, particularly for HEI settings. **Second**, we demonstrate and quantify significant spatiotemporal variability of indoor $PM_{2.5}$ concentrations at the building level. Our hourly $PM_{2.5}$ concentration time series reveal substantial variations throughout the day across different zones within the same building, creating potential exposure disparities among occupants. This high-resolution, room-level modelling is essential for informing building design and operational management, as it captures the distinct pollution levels experienced by individuals within the same facility. **Third**, we address a critical gap in understanding how building airtightness as a design standard affects outdoor air pollutant infiltration in HEI contexts. Given that data on HEI building envelope airtightness levels are scarce—representing a primary source of uncertainty in building simulation—we systematically vary Q_{50} to show this critical parameter's influence on infiltration rates and indoor $PM_{2.5}$ levels. **Fourth**, we developed a high-resolution IAQ-Energy model that captures spatial variability in infiltrated $PM_{2.5}$ concentrations during the heating season. This approach is particularly relevant for UK HEI buildings, where heating policies regulate indoor temperature based on outdoor conditions. Our coupled IAQ-Energy multizone simulation captures the dynamic interplay between temperature differences and $PM_{2.5}$ concentrations, advancing beyond previous models such as the UK Classrooms Archetype Stock Model (Schweizer et al., 2021), which employed thermal zones but neglected detailed airflow networks and spatial pollution variability

Our study's findings, while based on a specific HEI building stock in Sheffield, UK, provide a robust methodological framework and crucial insights that are broadly applicable globally. The high-resolution multizone air-thermal co-simulation approach using CONTAM and EnergyPlus is a validated and transferable methodology. This framework can be readily applied to HEI buildings in other countries and climate zones by adapting local input parameters such as weather data (.wth, .epw files), ambient air quality data (.ctm files), building envelope airtightness (Q_{50}), and specific internal heat gain benchmarks, as detailed in our methodology [66, 74, Table S1]. The coupling of CONTAM and EnergyPlus has been validated in various studies for different building types and pollutants. The fundamental challenges of balancing energy efficiency goals (e.g., increased airtightness) with maintaining good indoor air quality (IAQ), and the health risks associated with $PM_{2.5}$ infiltration, are universal concerns in buildings worldwide. Our findings underscore the importance of addressing these issues in any climate zone or country.

The observation of significant spatiotemporal variability of indoor $PM_{2.5}$ concentrations within buildings and the impact of building airtightness on infiltration rates and I/O ratios are fundamental principles that would manifest in HEI buildings globally. While the exact magnitudes would vary based on local outdoor pollution levels, climate, building codes, and construction practices, the analytical framework and the highlighted importance of high-resolution, coupled simulations for complex building typologies like HEIs remain highly relevant for assessing and improving indoor air quality performance across diverse contexts. Thus, our co-simulation approach, high spatial resolution, and analysis of spatiotemporal variability represent significant advancements, providing a robust and transferable framework for IAQ assessment in HEI buildings worldwide.

3. Review of building simulation for assessing IAQ

In building simulation for assessing IAQ, the way indoor airspace is partitioned to provide a required level of spatial detail can be summarised in three approaches: (1) a single and well-mixed zone, (2) multiple well-mixed zones, and (3) non–uniform distribution of the pollutants with Computational Fluid Dynamics (CFD) (**Figure** 1). Determining best models is nontrivial, often depending on the

modelling and simulation requirements, such as building complexity, the parameters investigated, the expected results, and the degree of accuracy required (Yu et al., 2019). A wide range of input parameters is required to perform IAQ simulations, including climate data, building fabric and geometry, building systems, and occupancy schedules (Persily & Ivy, 2001).

Assuming homogeneous physical properties of air (i.e. uniform temperature, air pressure, and contaminant concentrations), well-mixed single-zone models typically take a macroscopic view of air within one volume represented by a node. Meanwhile, multizonal models define multiple nodes (or zones), each node representing a room, or a group of rooms connected by several airflow paths. In both models, the airflows between each zone and the outdoor air are calculated iteratively using the mass balance equation (**Eq. 1**, Nazaroff, 2004), until the pressure relationships are solved at each time step.

$$\frac{\mathrm{d}(C_i V)}{\mathrm{dt}} = E + C_o[Q_s(1 - \eta_s) + Q_N + Q_L P] - C_i[Q_F \eta_F + \beta V + (Q_s + Q_N + Q_L)] \qquad (\textbf{Eq}.\ 1)$$

Where V is room volume (m^3), C_o is the concentration of particles in outdoor air ($\mu g/m^3$), C_i is the concentration of particles in indoor air ($\mu g/m^3$), Q_S is the mechanical supply flow rate (m^3/h), Q_N is the natural ventilation flow rate (m^3/h), Q_L is leakage (infiltration) flow rate (m^3/h), η_S is a filter with single-pass removal efficiency, P is the penetration fraction of particles, Q_F is indoor air particle control flow rate (m^3/h), η_F is a filter with single-pass removal efficiency, E is an emission source operating at ($\mu g/h$), and β is the loss of particles from indoor air by deposition represented by a first-order loss-rate coefficient (h^{-1}). The equation may be extended to include different processes when the indoor environment under study is represented as multiple well-mixed zones. This includes terms that account for the supply and loss of particle attributes by inter-zone and infiltration airflows (Miller & Nazaroff, 2001).

Computational fluid dynamics (CFD) modelling takes a microscopic view of airflow in a zone or a group of zones within a building (Yu et al., 2019). CFD models are particularly relevant where uniform mixing within a zone or zones cannot be assumed reasonably to represent the airflow conditions under investigation (Shimada et al., 1996). CFD-based models can compute fine- grained indoor contaminants concentrations and personal exposures, and they have been widely used to simulate contaminants infiltration from outdoor generated sources and contaminants transport between zones within a building (Panagopoulos et al., 2011).

To achieve reliable predictions of IAQ at multiple spatial and temporal resolutions, simulation tools need to be built with indoor particle dynamics mathematical models that capture the complex physical and environmental phenomena as accurately as possible. State-of-the-art IAQ models include multizone or airflow networks and CFD models. These models can calculate indoor air properties such as indoor air temperatures, airflow rates, and indoor contaminant concentrations. In predicting a building's IAQ, airflow network and CFD models perform differently in complexity, reliability and accuracy. CFD-based models are computationally expensive as they often resolve airflow dynamics at high spatial and temporal resolutions. Yet, Hensen and Lamberts (2011) pointed out that there appeared to be a widespread misconception that using CFD will reduce uncertainties and increase the accuracy of IAQ predictions. Deviating from the ideal case to higher or lower complexity can induce risks of simulation errors. Therefore, the selection of appropriate computation methods should be guided by the purpose of the simulation.

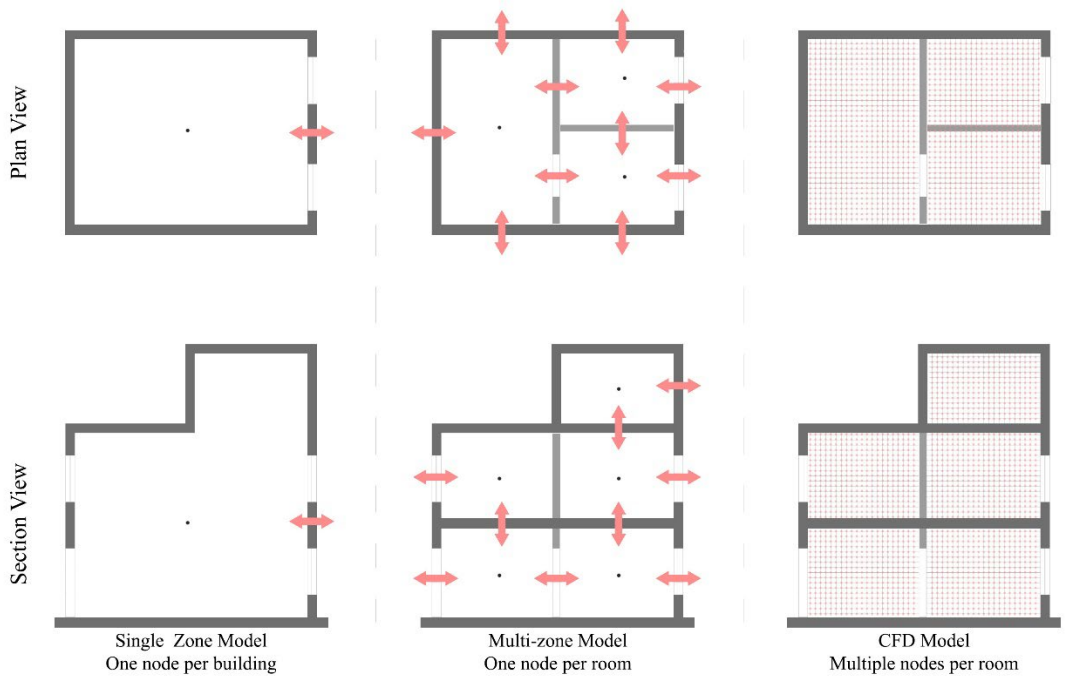

Figure 1: Approaches to IAQ modelling. Left: Single zone models; Middle: Multizonal models; Right: CFD Models. Each node represents a well-mixed volume. (adapted from Axley, 2007)

Both single-zone and multi-zone models assume of perfectly homogeneous or *well-mixed* conditions (i.e., each zone has an average air pollutant concentration value). In single-zone models, a building is simplified to be represented by a single zone or node without considering its interior partitions (Megri & Haghighat, 2007). Consequently, the physical details of heat and mass transfer between rooms within a building caused by temperature and pressure variations are ignored (Yu et al., 2019). **Figure 2** illustrates the assumptions, showing the air temperature in a single-zone model represented by an average value of T_{in} (°C) (Megri & Haghighat, 2007). A steady state model (**Eq. 2** & **Eq. 3**) stipulates that the mass flow rate $\dot{m}_{in}$ (kg/s) should be equal to the outlet mass flow rate $\dot{m}_{out}$ (kg/s) when infiltration is neglected, and the energy is conserved between $\dot{q}_{in}$ (rate of heat energy supplied into room/building (Watts), $\dot{q}_{out}$ (rate of heat energy removed from room/building (Watts), and $\dot{q}_{loss/gain}$ (rate of heat energy transferred through room/building structures (Watts).

$$\frac{dM_{space}}{dt} = \dot{m}_{in} - \dot{m}_{out} = 0 \qquad \textbf{(Eq. 2)}$$

$$\frac{dQ_{space}}{dt} = \dot{q}_{in} + \dot{q}_{out} + \dot{q}_{loss/gain} = 0 \qquad \textbf{(Eq. 3)}$$

Additionally, a single node represents the outdoor climate, and the physical parameters of this node are assigned from weather conditions. Notwithstanding, single-zone well-mixed models are relatively easy to implement and fast to compute. They are suitable for estimating bulk airflow properties when the domain of interest can be treated as a single zone or node.

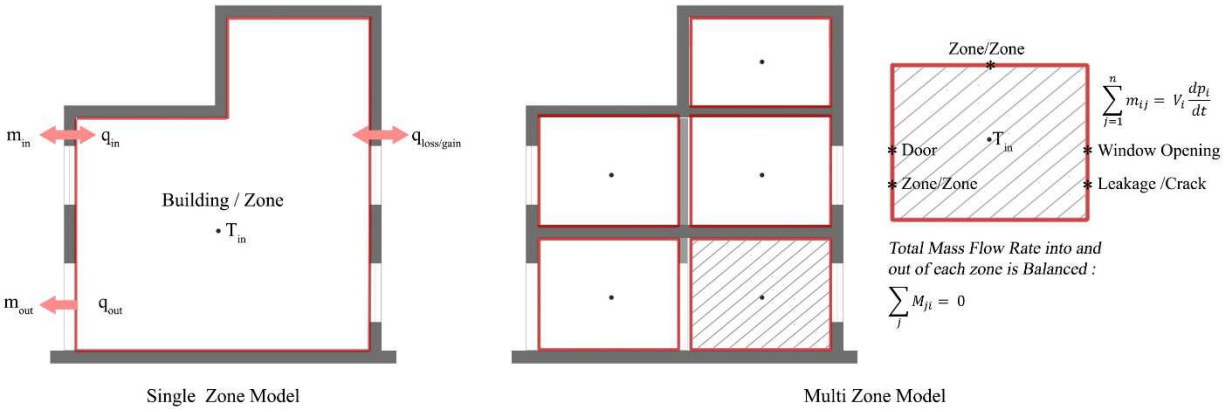

Figure 2: A summary of IAQ simulation assumptions of single-zone steady-state and multi-zone models. (Red lines delineate the inner volume of a zone (based on Yu et al., 2019)

Multi-zone models use rooms as the minimum computational unit. They calculate the airflow and contaminant transport inside a building within minutes or seconds. However, shorter computing times can be achieved by assuming homogeneity in each zone; that is, the distributions of air pressure, air temperature, and contaminant concentration in each room are assumed uniform and leave out the air momentum effect from an inflow opening (Axley, 2007). This is not always the case because a vertical temperature gradient exists in rooms filled with stratified flows driven by displacement ventilation or water heating systems (Wang & Chen, 2007). In addition, the well-mixing assumptions could be problematic for simulations of poorly mixed air and contaminants. In an earlier review of airflow and infiltration models, (Haghighat, 1989) stated that a multi-zone airflow model should be able to fully account for the driving forces that cause air to flow from outdoor to indoor and between indoor zones, including the stack effect, the wind pressure effect on building envelope, and the effect of HVAC systems on airflow.

In general, multi-zone airflow models are based on constructing a matrix of equations representing all airflow paths connecting zones (nodes) within a building. A mathematical equation describing each airflow path (i.e. door, window, crack, etc.) is used to numerically solve the resulting matrix, typically by the Newton-Raphson method (Conte & de Boor, 1972). All equations are solved iteratively to ensure reaching the convergence state when the sum of all mass flow rates through all flow paths approaches zero, as illustrated in **Eq. 4**.

$$\sum F_{ji} = 0 \qquad \textbf{(Eq. 4)}$$

where F_{ji} is the mass airflow rate from zone j to zone i (kg/s).

In a multi-zone model, the mass airflow rate at each airflow path is some function of the flow pressure drop along the flow path, P_j-P_i, and is expressed as:

$$F_{ji} = f(P_j - P_i) \qquad \textbf{(Eq. 5)}$$

The mass of air, m_i (kg), in zone i is given by the ideal gas law:

$$m_i = \rho V_i = \frac{P_i V_i}{R T_i} \qquad \textbf{(Eq. 6)}$$

Where ρ is the air density, V_i is the zone volume (m^3), Pi is the zone pressure (Pa), T_i the zone temperature (K), and R is the gas constant for air = 287.055 (J/kg.K).

Over the past decades, several IAQ simulation tools have been developed, such as Conjunction of Multizone Infiltration Specialists (COMIS) and CONTAM models (Feustel, 1999; Walton & Dols, 2005). These tools have been used primarily in modelling the IAQ of individual buildings of various types. CONTAM is a multi-zone airflow and contaminant transport simulation tool developed and maintained by the National Institute of Standards and Technology (NIST) (Dols & Polidoro, 2015). CONTAM has been extensively validated across a wide range of applications, including airflow, contaminant transport, natural ventilation, smoke movement, and integrated energy-IAQ simulations (Haghighat, 1996; Emmerich & Hirnikel, 2001; Fine & Touchie, 2021). CONTAM was developed with an updated version of the AirNet model (Walton, 1989) and provides a simple graphical user interface for intuitive inputs of building zones, construction, airflow paths and other building elements (McDowell et al., 2003).

More specifically, CONTAM allows users to model airflow rates, including infiltration, exfiltration, zone-to-zone airflows driven by mechanical ventilation systems, wind pressures on the building envelope and buoyancy effects. CONTAM's contaminant dispersal model is an implementation of the Axley methods (Axley, 1988; Axley, 1987) and has been widely used in many studies to predict contaminant concentrations in buildings under multiple designs and retrofitting scenarios (García-Tobar, 2019; Underhill et al., 2018). However, as a standalone package, CONTAM does not modify zonal air density in response to environmental changes due to building interactions and occupant behaviours. Therefore, CONTAM does not have the capability to perform dynamic indoor thermal simulations on its own.

As one of the widely used whole building energy simulation engines, EnergyPlus (Office of Energy Efficient and Renewable Energy) simulates airflows in buildings using the multi-zone Airflow Network Tool, which is an airflow model based on the early versions of COMIS and AirNet. The Airflow Network Tool can simulate infiltration and exfiltration rates driven by indoor/outdoor pressure differences, ventilation mechanisms, building envelope permeability, and zone-to-zone airflows. Using EnergyPlus to model contaminant transport, Taylor et al. have developed the Generic Contaminant Model (GCM) tool, allowing users to model the behaviour of one specific pollutant within a building. GCM enables the modelling of dynamic thermal behaviour and single pollutant transport within one simulation package (Taylor et al., 2014). Polluto, another in-house tool developed at the University College London (UCL), also offers multiple contaminants transport modelling with EnergyPlus. **Table 1** presents a comparison between CONTAM and the UCL in-house IAQ tools.

Table 1: Comparison of IAQ simulation tools used in housing stock IAQ modelling.

	Simulation Tools		
	CONTAM	EnergyPlusGCM	EnergyPlusPolluto
Main Usage	Airflow rates, contaminant transport through airflow, and building occupant exposure	Energy analysis, thermal load simulation, airflow, contaminant transport	Energy analysis, thermal load simulation, airflow, contaminant transport
User Interface	Simple	Complex	Complex

Thermal Behaviour	Static [Dynamic if coupled with a thermal engine]	Dynamic	Dynamic
Contaminant Behaviour	Yes (A rich set of sources and sinks, including deposition and re-suspension)	No	No
Changes in Occupant Behaviour Consideration	Yes	Yes	Yes
Modelling of Pollutants	Multiple Pollutants	Single Pollutant	Multiple Pollutants
Air Leakage Points	Multiple Airflow Leakage Points	A one-to-one correspondence between heat transfer and air leakage	A one-to-one correspondence between heat transfer and air leakage
Mechanical Systems Modelling	Complex & Multiple Systems	One System	One System
Warm-up Days	No	Yes, to ensure any thermal capacitance values are representative of the zone.	Yes, to ensure any thermal capacitance values are representative of the zone.
The capability of building control operations	Yes	Yes, indoor concentrations as flags for ventilation system operation	No
Non-trace contaminants	Yes, already included in air density calculations.	Yes, if coupled with the Heat and Moisture Transport (HAMT) model.	Yes, if coupled with the Heat and Moisture Transport (HAMT) model.

More recently, a mathematical description of the energy balance equations of EnergyPlus and the mass balance of airflows in CONTAM was proposed by Dols et al., (2016). New and existing components and tools have been developed and modified to facilitate synchronising building geometric representations and dynamic data exchange between CONTAM and EnergyPlus. The coupling of CONTAM and EnergyPlus enables simultaneous simulation of energy flows and air contaminant transport. This is significant as energy efficiency measures (e.g., reduced ventilation) can impact IAQ, and vice versa. CONTAM's ability to model the transport of pollutants (e.g., CO_2, VOCs, $PM_{2.5}$, PM_{10}) within a building is integrated with EnergyPlus thermal and energy calculations. This allows for detailed assessment of occupant exposure to pollutants. A more detailed account of CONTAM-EnergyPlus co-simulation workflow applied in this study is provided in **Section 4.2**.

To summarise, significant progress has been made in building simulation for assessing indoor air quality over the past decade. More sophisticated integrated modelling techniques combining IAQ, thermal comfort and energy performance simulations have been developed. These models allow for a more comprehensive assessment of building performance, considering the complex interactions between airflow, temperature, humidity, and pollutant concentrations. However, in-depth studies of IAQ in higher education buildings are sparse (e.g., Erlandson et al., 2019; Lama et al., 2022; Abbaspour et al., 2023). In particular, the impact of building airtightness as a building design standard on infiltration of air pollutants from outdoor sources in the HE context is not well

understood. The remaining of the paper reports an investigation of indoor air-thermal coupled simulation (co-simulation) to assess $PM_{2.5}$ concentrations of a large cohort of indoor spaces across diverse space types sampled from an HE institution building stock.

4. Materials and methods

4.1 Data sources

There is high heterogeneity in HEI buildings in terms of sizes, functions, designs, constructions, and space uses. In this study, the building data sources were provided by the University of Sheffield Estates and Facilities Management (EFM) team. These sources include general building information and layouts, HVAC systems in use and operational details, heating policies, lighting and appliances, building envelope construction details, U-values, occupancy schedules. Hourly weather and ambient air quality datasets were sourced from nearby local monitoring stations.

Five buildings were selected to represent the University of Sheffield building stocks of different construction ages 1920s-2000s (**Figure 3**). These buildings differ in size, geometry, construction methods and materials; thus, different building- related input parameters to model the IAQ were required. Moreover, HEI buildings tend to be composed of purpose-built spatial volumes (e.g., classrooms, student-led learning spaces, laboratories, staff offices etc.) connected by circulation routes, often resulting in large built areas exposed to external thermal and air flows. **Table 2** summarises the main characteristics of the selected buildings. Across the five buildings, a total of 2,729 zones (N =2,729) were identified for the co-simulation study.

The five case study buildings are all located on the main campus of the University of Sheffield in Sheffield city centre, UK. This urban environment is characterised by high density development with substantial vehicular traffic on adjacent major roads, including the A57 and A61). The area contains commercial and light industrial premises but lacks heavy industry or significant local point sources of industrial $PM_{2.5}$ emissions in the immediate vicinity.

Outdoor $PM_{2.5}$ concentrations for the simulation were obtained from the nearest urban air quality monitoring station (Sheffield Devonshire Green, UKA00575), located approximately 500 metres from the campus. This monitoring station captures the combined influences of urban background and traffic-related pollution, providing data representative of the outdoor environment experienced by the selected buildings. While the model does not explicitly resolve micro-scale pollution gradients or individual point sources, the monitoring station data adequately represent the campus environment and exposure context relevant to this study.

Given that UK law prohibits indoor smoking and no fuel combustion for cooking or heating is permitted on these HEI premises, we assume that indoor $PM_{2.5}$ concentrations result primarily from infiltration of outdoor sources. While minor indoor sources such as printers, human activities, and experimental equipment may contribute to $PM_{2.5}$ level, we excluded these from our analysis due to the lack of comprehensive, zone-level data on their presence and usage patterns across the diverse spaces modelled. This approach prevents the introduction of additional uncertainty into our simulation results while maintaining focus on the primary infiltration pathways that can be reliably quantified. The period of building simulation was performed during the heating season (Nov-Apr, 2019-2020), assuming little or none window-opening behaviour in these buildings. The poorest ambient air quality in England is typically observed during March and early April, with significant health impacts noted during this period (Gillian et al., 2015).

Figure 3: Buildings selected representing the HEI building stocks

Table 2: Summary of the features of the selected HEI buildings

Building	BH	ADC	AT	RC	ICS
Construction Period	1920s	1940s	1960s	1990s	2000s
Function	Offices, Seminar Rooms, and Meeting Rooms	Offices, Seminar Rooms, Meeting Rooms, and Open-office Style Study Space	Offices, Seminar Rooms, Meeting Rooms and Studios	Large Computer Rooms, Open-office Style Study Space, Lecture Theatres, Cellular Staff-Offices, and Meeting Rooms	Labs and Seminar Rooms
Distinctive Feature	Linear Circulation System	Compact Floor Layout with Compound Circulation	High-rise Central Core with Radial Circulation	Courtyard with Linear Circulation	Atrium Building
Refurbished	Yes	Yes	Yes	No	No
Height Classification*	Low Rise	Low Rise	High Rise	Low Rise	Mid Rise
Total Number of Floors Above Ground	2	2	20	3	5
Building Built-Up Area (m^2)	874.48	1,351.25	16,402.36	9,057.09	1,947.80
Cooling Method	Natural Ventilation W/ Exhaust System	Natural Ventilation W/ Exhaust System	Natural Ventilation W/ Exhaust System	Natural Ventilation W/ Exhaust System	Natural Ventilation W/ Exhaust System
Heating Method	Gas Fired Wet Heating System	Central Heating via Wall Mounted Radiators	Central Heating via Wall Mounted Radiators	Central Heating via Wall Mounted Radiators	Central Heating via Wall Mounted Radiators
External Walls	Solid Wall	Solid Wall	Double Glazed Curtain Wall System	Cavity Wall	Cavity Wall and Pre-painted Copper Sheets
External Walls U-Values ($W/m^2.K$)	1.80	1.80	2.20	0.60	0.45

*Height classification is defined as: Low Rise (1–3 floors), Mid Rise (4–7 floors), and High Rise (8 or more floors), based on the total number of above-ground floors for each building.

4.2 Methods and co-simulation tools

4.2.1 CONTAM-EnergyPlus coupling workflow

This study used deterministic values described by discrete or continuous probability distributions for the input parameters. Based on these input parameters, CONTAM and EnergyPlus can be used to estimate each zone's annual average infiltrated $PM_{2.5}$ concentrations. Quantifying the uncertainty in the outputs by systematically varying each set of CONTAM and EnergyPlus inputs and running multiple simulations was not within the scope of the study.

Figure 4 illustrates the relationship between the CONTAM and EnergyPlus components in coupled thermal, airflow and contaminant simulation. CONTAM's graphical user interface, ContamW, allows creating project files (.prj) representing scaled geometries of building floor plans. Contam3Dexporter tool creates an EnergyPlus input data file (IDF) (.idf) and files containing data exchange parameters (VEF and XML files). The IDF file can be edited and exported again using the SketchUp software plugin OpenStudio. Contam3Dexporter tool exports a Windows dynamic link library (ContamFMU.dll) based on the Functional Mock-up Interface (FMI) Co-Simulation specification version 1.0 (Blochwitz et al., 2011). ContamFMU.dll manages data exchange and the execution of ContamX during the co-simulation. At present, EnergyPlus transfers zone temperatures, ventilation systems airflows, outdoor airflow fractions, output variables, and outdoor environment data to ContamX. On the other hand, ContamX transfers zone infiltration rates, inter-zone airflows and control values. Previous studies have validated and verified this process (Emmerich et al., 2019). More recently, the application of the co-simulation approach has been part of several studies to estimate indoor $PM_{2.5}$ exposure profiles (Milando et al., 2022) and to perform a whole building analysis (IAQ, Energy, and Ventilation) (Dols et al., 2021).

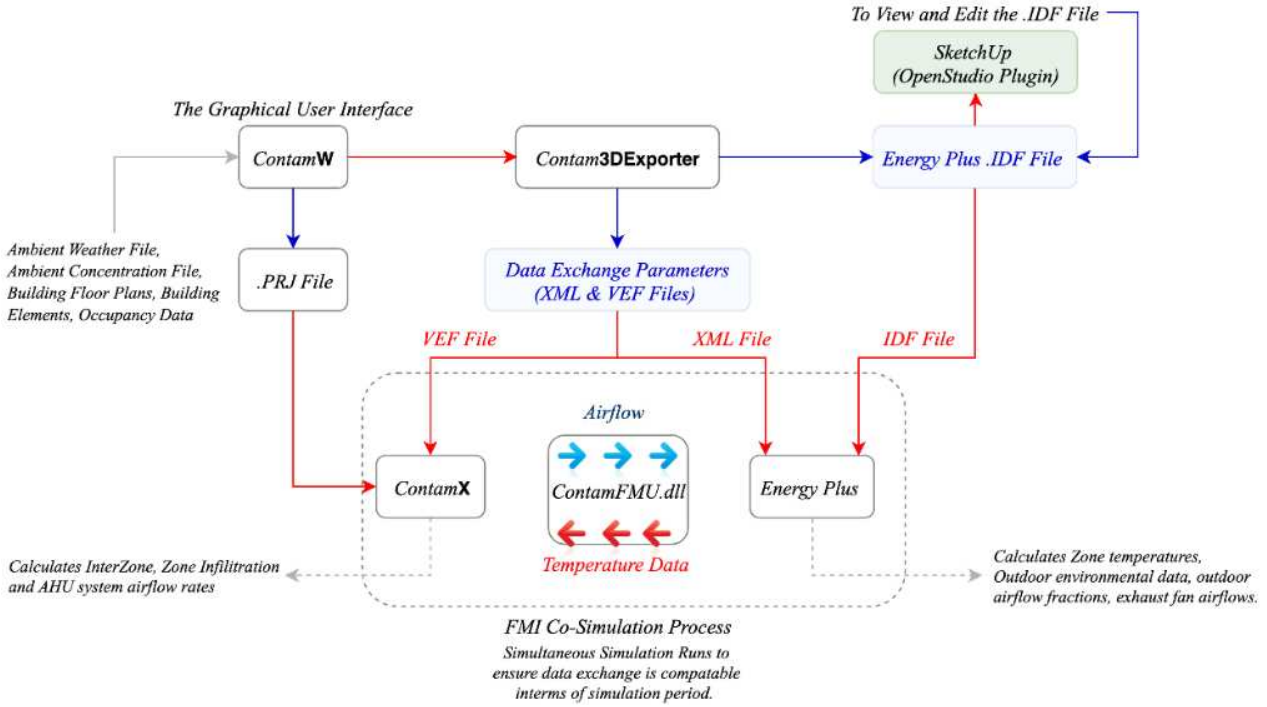

Figure 4: Schematic relationship between components of CONTAM and EnergyPlus in coupled airflow, contaminant and thermal simulation (adapted from Dols et al., 2016)

As an example, **Figure 5** shows the ADC building layout using ContamW (CONTAM graphical user interface). Each room/space (as labelled on the EFM CAD drawings) was considered a single volume to which doors connect all other rooms. After the rooms and doors were drawn, well-mixed zones and airflow paths (represented as diamond-shaped dots) were mapped. A fundamental assumption in using ContamW is that the modelling must capture the (a) juxtaposition of zones to account for inter-zone flows, (b) zone volumes to account for contaminant dilution, and (c) wind pressure coefficients to account for the effect of wind on the building envelope. Each CONTAM model was drawn using the pseudo-geometry option to define the scaling factor for drawing and viewing the wall, zone and duct dimensions.

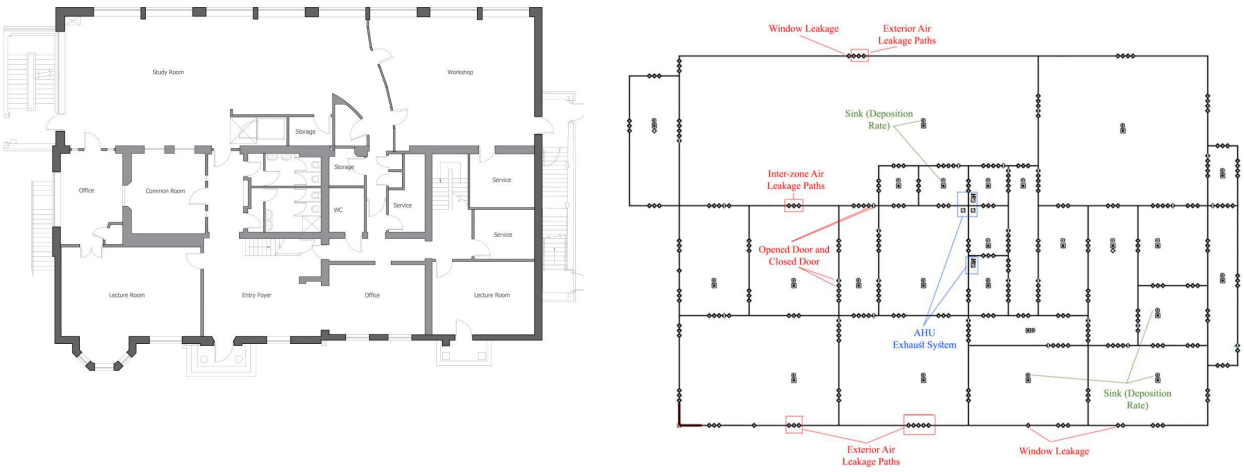

Figure 5: CONTAM elements of the ADC building layout (ground floor)

4.2.2 Airflow paths

Each zone has a variable volume and floor area resulting in variable airflow paths. Airflow paths (in red) and sinks (in green) are identified for each zone, and exhaust systems (in blue) in kitchens and toilets. Air leakage paths are modelled using a single graphic element to represent potential airflows through walls and windows. Three airflow paths are used to model air leakage paths in each external and internal wall of a zone, which is assumed to be uniformly porous, by locating at its top, midpoint, and bottom following (Jones et al., 2013). An exhaust fan is linked to a central AHU unit for each floor to account for potential airflows in kitchens and toilets. This information can be acquired by accessing the EFM's mechanical CAD drawings for each building. The process of identifying all air leakage paths was similar for all buildings.

To match the calculated airtightness level normalised by thermal envelope area Q_{50} ($m^3/h/m^2$) with the values provided in **Table 3**, The effective leakage area at 4Pa ELA_{4pa} (cm^2/m^2) was used as an input in ContamW and is represented by the following (**Eq. 7**):

$$ELA_{4Pa} = \sqrt{\frac{\rho}{2(4Pa)}} \times Q_{50}\,(4Pa/50Pa)^n \qquad \textbf{(Eq. 7)}$$

Table 3: Baseline airtightness Q_{50} values for the five selected buildings

Building	Airtightness Q_{50}	Construction Year	Reference
Building 1 (BH)	13 $m^3/h/m^2$	1920s	-
Building 2 (ADC)	13 $m^3/h/m^2$	1940s	-

Building 4 (AT)	10 $m^3/h/m^2$	1960s	HLM Architects
Building 3 (RC)	10 $m^3/h/m^2$	1990s	CIBSE TM23
Building 5 (ICS)	7 $m^3/h/m^2$	2000s	CIBSE TM23

Where ELA_{4Pa} is the effective leakage area at 4 Pa (cm^2/m^2), n is the dimensionless flow exponent, and ρ is the air density (kg/m^3). The value of the flow exponent n ranges from 0.5 for large openings and 1 for small ones. Previous studies in the US suggested that n can be sampled from a normal distribution N (0.651, 0.077) (Sherman & Dickerhoff, 1998) and between 0.6-0.7 for typical infiltration openings (Dols & Polidoro, 2020). In the absence of similar UK studies for non-domestic buildings, n was assumed to follow the same normal distribution in this study and was assigned the value 0.65. Here, windows were modelled with the assumption that they were all closed during the heating season as per the EFM heating policy. However, to account for the air leakage of windows, they were modelled in ContamW using **Eq. 7**. and were assigned a leakage value representing the total leakage value for an item (cm^2). The discharge coefficient Cd was 0.6 as per the CONTAM User Guide (Dols & Polidoro, 2020).

Airflow and the transfer of pollutants and thermal energy can occur between different zones within a building or between inside and outside environments through other large openings like open doorways. These airflows tend to be more intricate, with the possibility of airflows in opposite directions in various parts of the opening. Two models, the *two–way flow one–opening* model and the *two–way flow two–opening* model, can be used to study such airflow in CONTAM (Dols & Polidoro, 2020). The former considers the flow through a single large opening and defines the neutral plane level (NPL) where the air velocity is zero. The NPL is the height at which the internal pressure equals the external pressure, resulting in no airflow in or out of an opening at that height. Above or below the NPL, the airflow and direction can be determined, with vents positioned below the NPL acting as inlets and those above acting as outlets, or vice versa.

The latter model divides an opening vertically and uses two power-law models to estimate the net flow rate in each direction, accounting for the two-way flow due to the stack effect over the height of a tall opening (Walton, 1989). The concept of the NPL is helpful in building design and is referenced in design standards such as the CIBSE AM10 guide (CIBSE, 2005). For simplification, open internal doors were modelled using the two–way flow one–opening model, with a discharge coefficient of 0.78, and its relative elevation is at the bottom of the door. When closed, doors were modelled as leakage elements that represent the door undercut given in (cm^2). Finally, simulations of a blower door test at 50 Pa were run in CONTAM for each building to ensure that the model's external air leakage rate (Q_{50}) was correct (**Table 4**).

Table 4: Summary of the used Effective Leakage Areas ELA_{4Pa} for external and internal walls elements to achieve the airtightness level $\mathbf{Q_{50}}$ using CONTAM's blower test at 50Pa

Leakage Level	Airtightness Level Q_{50} ($m^3/h/m^2$)	External Wall and Internal Walls ELA_{4Pa} (cm^2/m^2)
Tight Building Envelope	3	0.925
	5	1.550
	7	2.155
	9	2.775
	10	3.075
	11	3.375
Leaky Building Envelope	13	3.997

The Q_{50} values applied in this study reflect CIBSE TM23 benchmarks for non-domestic buildings and observed ranges in UK literature (CIBSE 2022). While HEI-specific airtightness data remain limited, the parametric analysis across a realistic Q_{50} spectrum ensures broad applicability to HEI building stocks with varying envelope conditions. We acknowledge the need for standardised HEI airtightness data collection and endorse this as a priority for future research. The model's framework can be refined as such data emerge.

4.2.3 Local weather and ambient air quality conditions

To account for the local weather conditions during the 12 months of 2019 selected for this study, the weather data from the nearby automatic weather station was converted into CONTAM's weather data format (.wth) (Dols & Polidoro, 2020). Data is reported hourly, giving the date and time, ground temperature, atmospheric pressure, wind velocity, wind direction, and absolute humidity. The same weather file was used in the simulations for all selected buildings.

According to the $PM_{2.5}$ data downloaded from the local air quality monitoring station (UKA00575), **Figure 6** shows that during the winter months, the levels of $PM_{2.5}$ peaked in February and April with an average monthly level of 20.49 and 23.11 µg/m^3, respectively. On the other hand, the monthly outdoor $PM_{2.5}$ between May and October ranged from 10.61 to 6.41 µg/m^3. When comparing the seasonal outdoor $PM_{2.5}$, it can be seen in **Figure 7** that in the heating season (November to April), the average seasonal outdoor $PM_{2.5}$ level is 17.04 µg/m^3, which is higher than the WHO annual average permissible level of 10 µg/m^3. Meanwhile, in the non-heating season (May to October), the average seasonal $PM_{2.5}$ was 6.78 µg/m^3. This suggests the importance of monitoring indoor $PM_{2.5}$ infiltrated from outdoor sources during heating months.

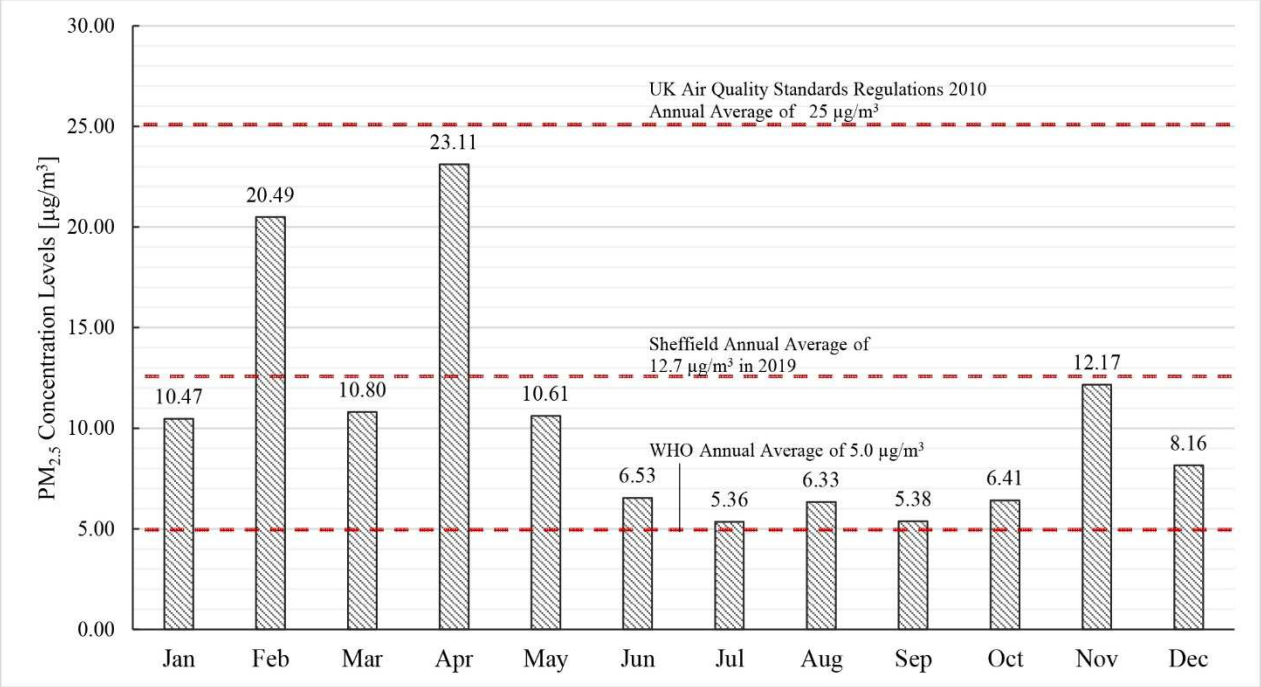

Figure 6: Monthly average outdoor $PM_{2.5}$ concentrations in Sheffield in 2019 (https://uk-air.defra.gov.uk/)

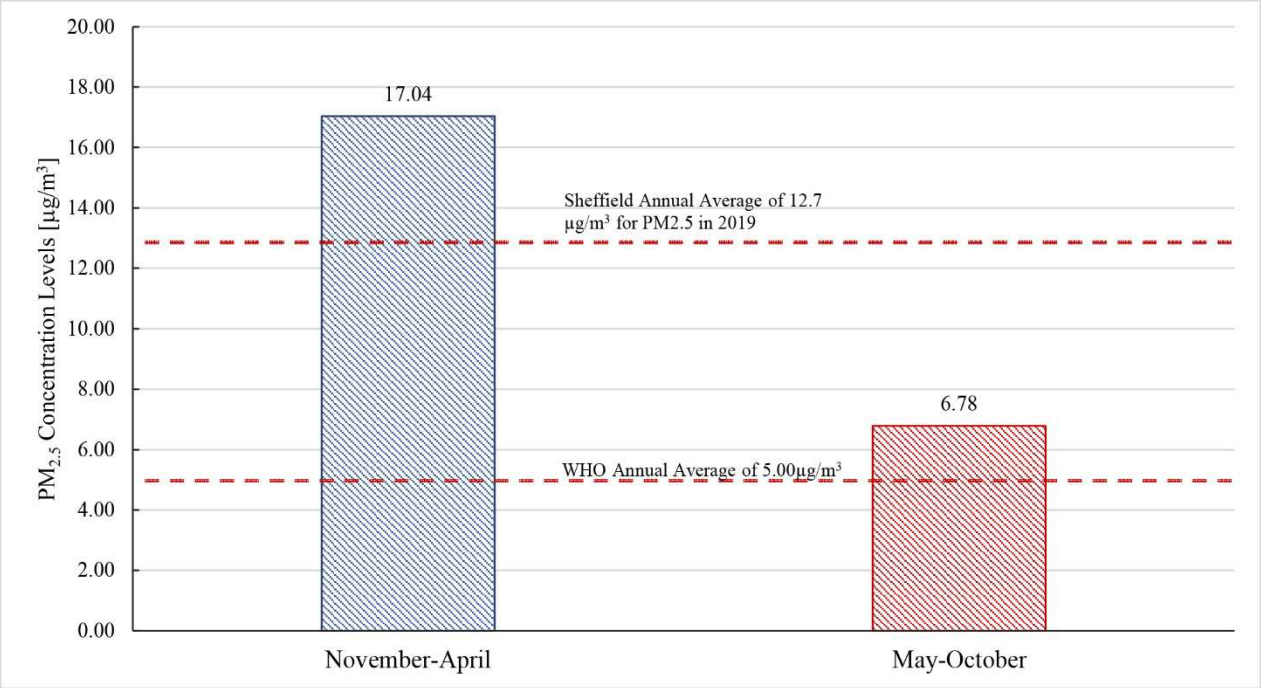

Figure 7: Comparison between the Heating season (Nov-Apr) and Cooling (Non-Heating) season (May-Oct) outdoor $PM_{2.5}$ concentrations (https://uk-air.defra.gov.uk/)

To account for the local wind effects on each side of the buildings, the wind effects were estimated using a wind pressure profile calculated using wind pressure coefficient (C_P) relationships found in (Swami & Chandra, 1987). Wind pressure profiles for each building are a function of the block aspect ratio (S) and the terrain constants. A variable wind speed modifier corresponding to "urban" terrain and scaled to building height (Dols & Polidoro, 2020), was applied to all exterior leakage paths. This parameter was used in CONTAM to account for the effects of local terrain on wind speed variation with height above ground level (**Table 5**).

C_P at different angles were assumed to be between 0◦ to 360◦ and specified for each side of the building. As the building form can significantly differ between the selected buildings, it can impact the resultant wind effects. Due to the lack of other resources that may represent such heterogeneous forms, the uncertainty in the resultant wind pressure profiles using the Swami and Chandra model is acknowledged.

Table 5: Building Heights, Local Terrain Constant, Velocity Profile Exponent, and Corresponding Wind Speed Modifier input data applied in CONTAM

Building Label	Building Height (m)	Local Terrain Constant	Velocity Profile Exponent	Wind Speed Modifier
Building 1 (BH)	6.0			0.410
Building 2 (ADC)	7.5			0.453
Building 3 (RC)	13.4	0.717	0.22	0.581
Building 4 (AT)	72.0			1.165
Building 5 (ICS)	21.8			0.718

4.2.4 $PM_{2.5}$ deposition rates

Deposition rates are essential in determining the removal rates and indoor concentrations of pollutants, especially when ventilation is limited. Here, the deposition of $PM_{2.5}$ was modelled as a

deposition rate sink model with a constant value of k =0.39 h^{-1} (**Table 6**). This simplification was necessary due to the absence of zone-specific data on furniture density, surface-to-volume ratios, or air velocity profiles across the 2,729 zones modelled. Nevertheless, this value was considered uncertain due to several factors such as room dimension, furniture area, and air velocity. Although all these parameters change by building/zone, this study took a simplified approach to the deposition process and input values (Nazaroff & Cass, 1987).

Table 6: Physical and behavioural properties of $PM_{2.5}$ used in this study

Pollutant	Molecular weight (g/mol)	Mean Diameter (μm)	Deposition Rate (h^{-1})	Penetration Factor P
Particulate Matter $PM_{2.5}$	1.4	2.50	0.39 (±0.16)	P = 0.8 (Infiltration), P = 1 (Natural Ventilation)

4.2.5 Indoor temperatures

As CONTAM is not a thermal model, the internal air temperatures must be specified as constant values for each zone. However, to account for the dynamic interaction between thermal flow and airflow within a building, CONTAM can be coupled with EnergyPlus following the framework given in (Dols et al., 2016). In generating the CONTAM project file (.prj) for each building, a constant indoor temperature of 21°C was used. This temperature represents the heating season setpoint specified in the EFM heating policy. This allows ContamX to calculate initial infiltration rate values that can be used as dynamic infiltration flows rather than constant values. Then, CONTAM3DExporter was used to export EnergyPlus IDF files from COMTAM PRJ files. The IDF file contains all data exchange parameters representing the geometry of each building. The exported IDF files were manually edited for each building to include the thermal-related input parameters. This includes the thermal properties (U-Values) of the building construction, adding windows to account for the heat gain from solar radiation, identifying sources of internal heat gains and occupancy schedules, and the design of the Veolia DHN informed by the EFM.

Table 7 summarises benchmark allowances of the sensible and latent heat loads for different space types, assuming an indoor temperature of 21°C and a sedentary occupancy activity level (CIBSE, 2018). Occupancy density for each space type (m^2/person) was used to calculate the total number of occupants and the total occupants' heat gain for each zone.

Table 7: Summary of the benchmark allowances for internal heat gain from occupants, artificial lighting, and equipment in different space types (Source: CIBSE, 2018)

Building Type	Use	Floor Area (m^2/person)	Sensible Heat Gain W/m^2			Latent Heat Gain W/m^2	
			People	Lighting	Equipment	People	Other
Offices	Cellular Office	9	10	8-12	25	7.5	-
	Shared Office	4.5	20	8-12	20	15	-
	Meeting Rooms	3	27	10-20	5	20	-
Education	Lecture Theatres	1.5	67	12	2	50	-
	Computer Spaces	2.5	53	12	60	40	-
	Seminar Rooms	3	27	12	5	20	-

A summary of the input parameters of CONTAM(.prj) and EnergyPlus (.idf) is provided in the supplementary table (**Table S1**).

4.2.6 Co-simulation outputs and processing

After the co-simulation files were built for the selected buildings, simulations were run for a whole year. Generally, the shorter the time step, the more accurate the solution is, but at the expense of computational resources and runtime. Due to the sensitivity of the time step selected in the analysis of indoor $PM_{2.5}$ and its behaviour in indoor environments compared to other building-related performance analyses (e.g. annual energy use) (Tabares-velasco, 2013), a time step of 4 per hour (i.e., 15-min interval) was set in both CONTAM and EnergyPlus. The resultant airflow calculations, pollutant behaviours, and building envelope thermal responses can be modelled more accurately. In CONTAM, concentrations are reported at a moment in time and only according to the "Output" time step, regardless of the "Calculation" time step identified in the simulation settings.

The co-simulation process was repeated using the seven airtightness values specified (see **Table 4**) and assuming that windows are closed during the heating season (November–April) and open during the non-heating season (May–October). In addition, any mechanical ventilation systems were switched off (except extract fans in toilets and kitchens) during the co-simulation. Thus, the total airflow rate ACH_T (h^{-1}) was assumed to equal the simulated infiltration rate ACH_{INF} (h^{-1}).

In post-simulation processing, each zone's average concentration of infiltrated $PM_{2.5}$ during the heating season was calculated over the simulation period. Next, using the building operation period (7 AM-7 PM), the average concentrations in each room were weighted using the 12-hour occupancy time. Then, the time–series data of the infiltration rates ACH_{INF} (h^{-1}) for each zone, the infiltrated $PM_{2.5}$ concentrations ($\mu g/m^3$) for each of the zones, the outdoor scaled wind speed (m/s), and the indoor temperature T_{in} (◦C) were obtained. Finally, the simulated ACH_{INF} and $PM_{2.5}$ were extracted from the CONTAM output files, and ΔT was computed using the EnergyPlus time-series indoor temperature (T_{in}) value and the weather data.

4.2.7 Statistical methods

The study utilised a range of quantitative analyses to process and interpret the simulation outputs. (1) Descriptive statistics, including averages (mean), median, minimum and maximum ranges, standard deviation (SD), and variance, were extensively used to quantify hourly, seasonal, and annual concentrations of infiltrated $PM_{2.5}$, as well as infiltration air change rates (ACHINF) and indoor/outdoor (I/O) ratios across 2,729 zones. (2) For relational analysis, the determination coefficient (R-squared, R^2) was applied to assess the strength of the linear relationship between daily indoor and outdoor $PM_{2.5}$ concentrations, demonstrating, for instance, an R^2 of 0.89 for a zone with a Q_{50} of 7 and 0.85 with a Q_{50} of 3. (3) Distributional analysis employed Cumulative Distribution Function (CDF) plots to visualise the annual distribution of $PM_{2.5}$ concentrations across all simulated zones, allowing for the determination of the percentage of zones exceeding World Health Organization (WHO) $PM_{2.5}$ guidelines (e.g., 10 $\mu g/m^3$ and 5 $\mu g/m^3$) under various building airtightness (Q_{50}) settings.

While direct field validation was precluded by the COVID-19 pandemic, the study referenced the ASTM D5157-19 Standard Guide for Statistical Evaluation of Indoor Air Quality Models for validation methodology. This standard recommends using a correlation coefficient of 0.9 or greater, a regression line slope between 0.75 and 1.25 with an intercept less than 25% of the average concentration, and a Normalised Mean Square Error (NMSE) less than 0.25. An indirect validation for indoor temperature showed a correlation coefficient of 0.76 and an NMSE of 0.48, indicating some agreement with field measurements. These methods collectively allowed for the analysis of relationships between building parameters, such as airtightness, and indoor air quality outcomes.

5. **Results**

The outputs from the co-simulations yield four sets of results as presented below: (1) Simulated $PM_{2.5}$ hourly time series, (2) Average seasonable and annual concentrations of infiltrated $PM_{2.5}$, (3) $PM_{2.5}$ infiltrations under varying Q_{50} for all zones, and (4) $PM_{2.5}$ indoor/outdoor (I/O) ratios.

5.1 Hourly indoor $PM_{2.5}$ concentrations time series

With a 15-min temporal resolution, the simulated $PM_{2.5}$ concentrations and air change rates (ACH_{INF}) from CONTAM and the indoor temperature (T_{in}) from EnergyPlus were resampled to generate hourly averages for data analysis over the heating season. At the hourly resolution between 01 November and 30 April, the total number of data points for each zone was 4,344, totalling 1,941,768 data points across the 445 zones simulated. As an example of the time series outputs, Figure 8 shows the hourly indoor PM2.5 concentrations of four zones sampled from Building 3 (RCB), using the baseline Q_{50} of 10 m3/h/m2. These zones include a south-facing room located on 1st floor (Z30), a southeast-facing room on 2nd floor (Z122), a north-facing room on 1st floor (Z96), and a north-west facing room on 3rd floor (Z87).

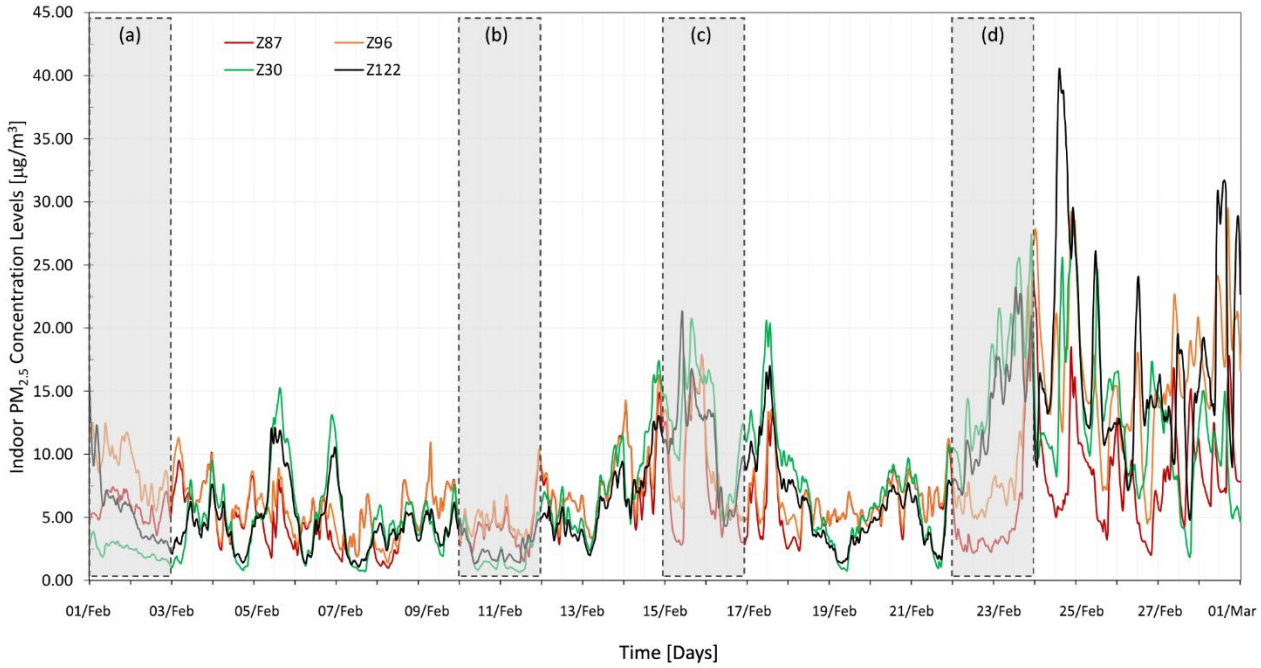

Figure 8: Simulated hourly indoor $PM_{2.5}$ concentrations in four different zones sampled from Building 3 (RCB), showing the spatial and temporal variability within the same building during 01 Feb – 01 March 2019. The Q_{50} of this building is 10 $m^3/h/m^2$.

Zooming into the (a), (b), (c), and (d) time bands in Figure 8, it can be seen in **Figure 9 (a-d)** that the concentrations of infiltrated $PM_{2.5}$ vary significantly throughout the day in different zones (rooms) within the same building. The spatial variability shown here is crucial as it could lead to exposure disparities among building users in different zones within the same building. As such, studying the causes of the spatial variability on indoor $PM_{2.5}$ can inform building design and operational management. This can only be achieved through constructing models of a high spatial resolution at the room level across the HE buildings. The extent of variability could be due to the mediating effects of environmental and building characteristics on the ingress of $PM_{2.5}$ from outdoor sources. This highlights the necessity of achieving a model resolution at the room level for assessing spatiotemporal variation of $PM_{2.5}$ infiltrations in complex HE buildings.

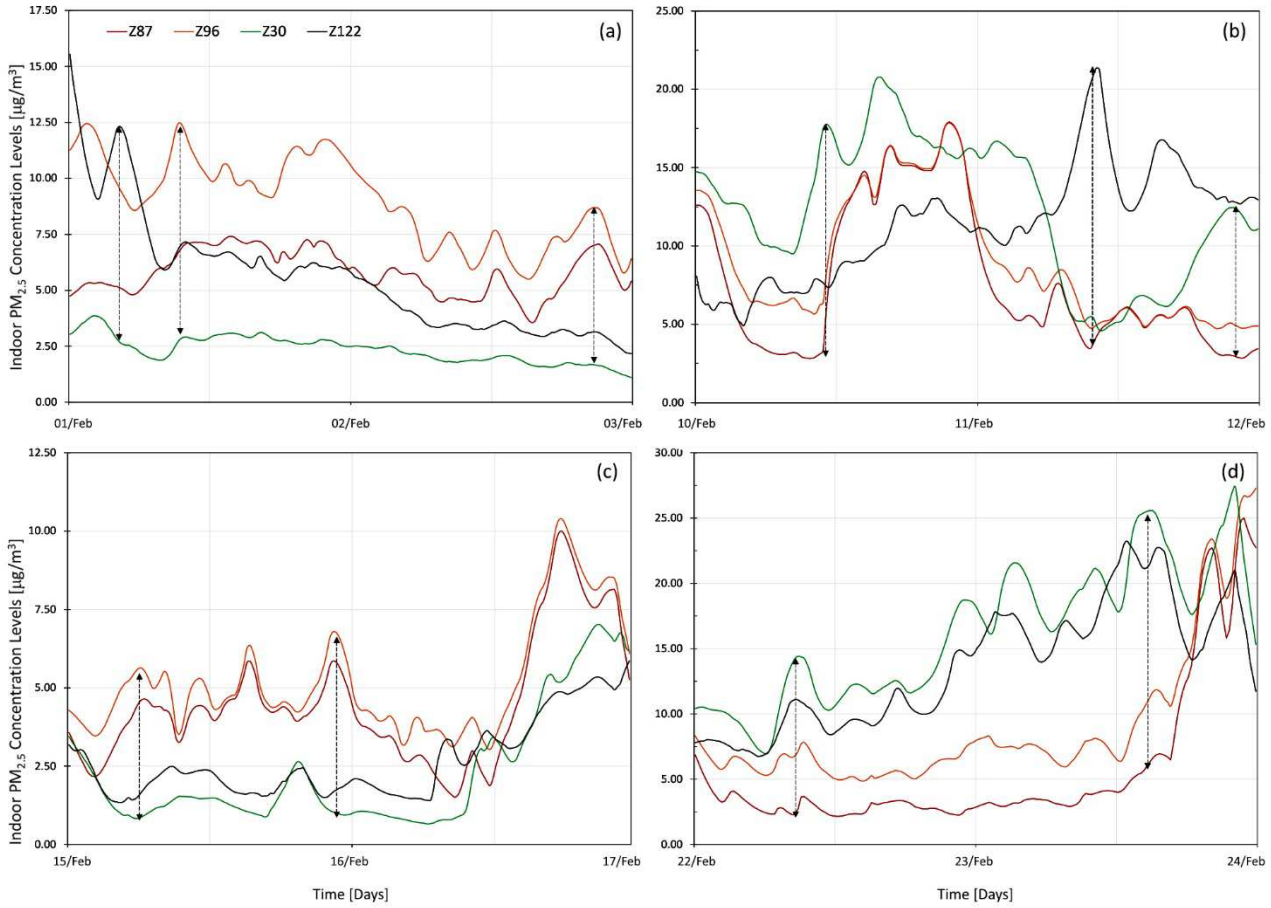

Figure 9 (a-d): Hourly indoor $PM_{2.5}$ concentrations in four different zones in Building 3 (RCB) showing the spatial (zone location) and temporal (black arrows ↔) variability of $PM_{2.5}$ concentrations within the same building.

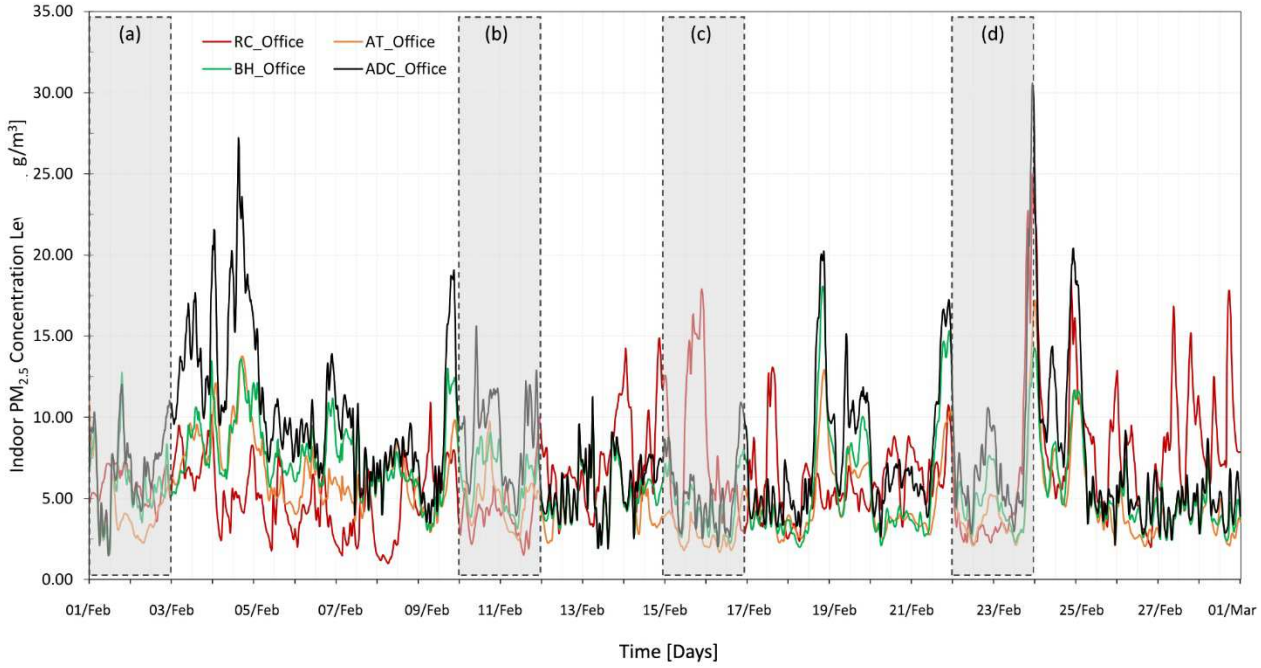

Figure 10: Simulated hourly indoor $PM_{2.5}$ concentrations of the office zones sampled from the four buildings

The hourly $PM_{2.5}$ concentrations series also reveal notable spatiotemporal variability across multiple buildings. **Figure 10** shows the hourly indoor $PM_{2.5}$ series of office zones sampled from four buildings using the baseline Q_{50}. These office zones include a south-facing room in Building 1 (BH), a north-facing room in Building 2 (ADC), a southeast-facing room in Building 4 (AT), and a south-facing room in Building 3 (RC).

Zooming into the four selected time bands, **Figure 11 (a-d)** shows the trends of infiltrated $PM_{2.5}$ concentrations during the selected timeframes. It can be noticed that the trends of infiltrated $PM_{2.5}$ vary throughout the day towards the end of the month when they exhibit a similar trend between 22-24 February (**Figure 10.d**). These time series outputs show that $PM_{2.5}$ in individual zones of the same space type (Office in this case) are sometimes similar in trend (overall peaks and troughs) but differ in location.

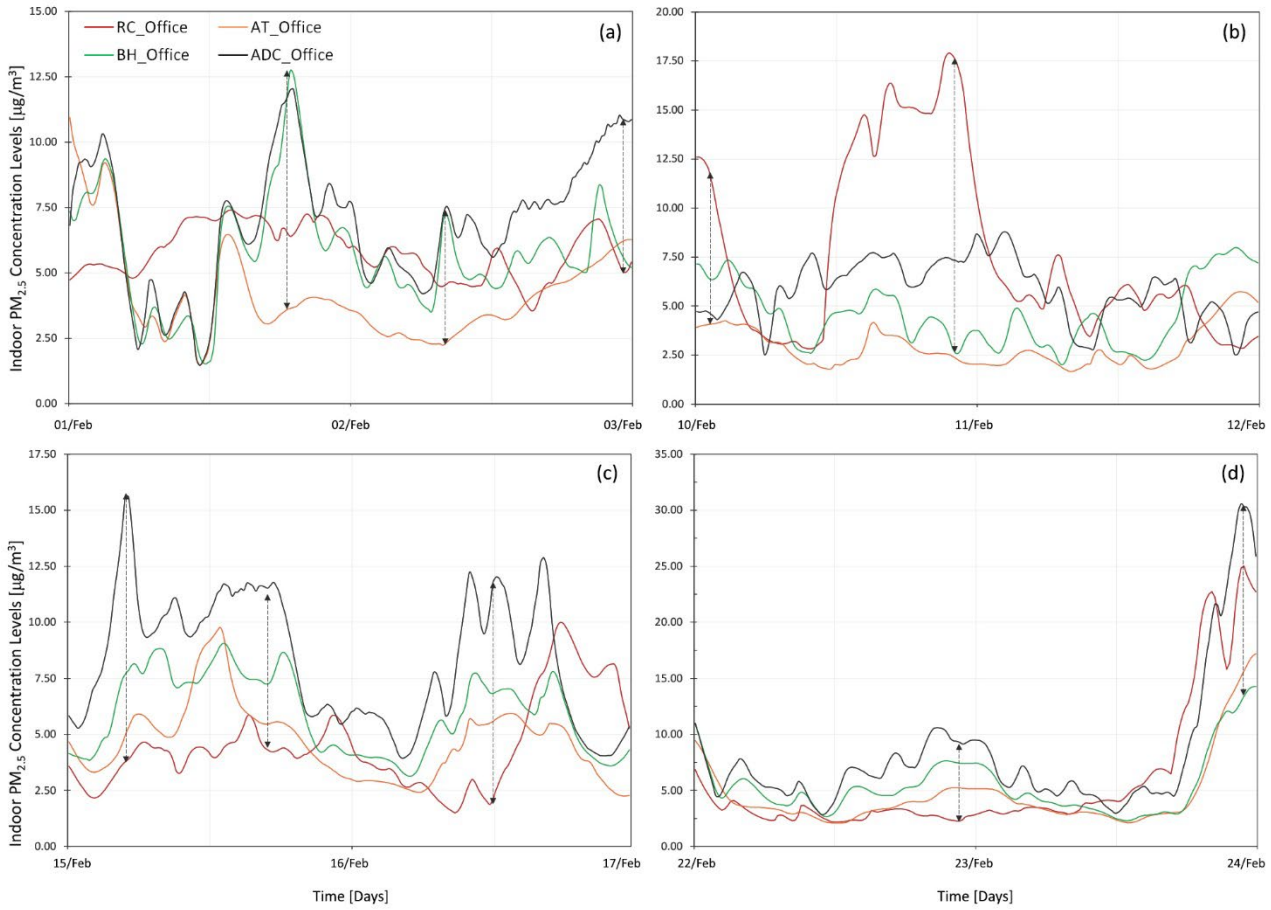

Figure 11 (a-d): Hourly indoor $PM_{2.5}$ concentration levels in the Office zones across four buildings during the four periods in February 2019 (black arrows ↔ highlighting the temporal variation)

5.2 Average seasonal and annual concentrations of infiltrated $PM_{2.5}$

To examine the relationships between infiltrated $PM_{2.5}$ and environmental and zone characteristics in a further study, the co-simulation outputs were resampled to generate average concentrations of infiltrated $PM_{2.5}$ over the heating season (Nov–April) and the year (annual). Although previous studies have reported that building characteristics (e.g., building type, age, and floor level) can influence indoor air quality, the building envelope airtightness Q_{50} can also play a role in building users' exposure to infiltrated $PM_{2.5}$ from outdoor sources. Quoting the Q_{50} baseline values (from

Table 3), the heating season concentrations and annual concentrations of infiltrated *$PM_{2.5}$* are summarised in **Table 8**.

Table 8: Descriptive statistics for the baseline concentrations of infiltrated $PM_{2.5}$ over the Heating Season and the (*Annual Average Concentrations*)

Building	Q_{50} ($m^3/h/m^2$)	Number of Zones	Min-Max $PM_{2.5}$ ($\mu g/m^3$)	Mean $PM_{2.5}$ ($\mu g/m^3$)	Median $PM_{2.5}$ ($\mu g/m^3$)	SD	Variance
BH	13	20	5.16-9.24 *(8.11-14.06)*	7.04 *(10.83)*	6.95 *(10.80)*	1.14 *(1.61)*	1.39 *(2.79)*
ADC	13	26	3.33-8.15 *(5.28-12.61)*	6.86 *(9.97)*	6.79 *(9.61)*	1.13 *(1.38)*	1.74 *(1.59)*
AT	10	185	3.63-9.39 *(5.59-13.82)*	6.02 *(9.02)*	5.96 *(8.85)*	1.02 *(1.42)*	1.06 *(2.04)*
RC	10	224	4.53-8.53 *(7.71-13.15)*	6.56 *(10.38)*	6.59 *(10.43)*	0.74 *(1.00)*	0.55 *(1.01)*

The annual concentrations estimated at the building level indicate the potential risks of long-term exposure to infiltrated $PM_{2.5}$ in these buildings. Building 1 (BH) exhibited an annual $PM_{2.5}$ concentration range of 8.11-14.06 µg/m³, with a mean concentration of 10.83 µg/m³. Building 2 (ADC) showed a slightly lower annual $PM_{2.5}$ concentration range of 5.28-12.61 µg/m³, with a mean concentration of 9.97 µg/m³, although they share the same Q_{50} (13 $m^3/h/m^2$). Building 4 (AT) had an annual concentration range of 5.59-13.82 µg/m³, with a mean concentration of 9.02 µg/m³. Building 3 (RC) demonstrated an annual concentration range of 7.71-13.15 µg/m³, with a mean concentration of 10.38 µg/m³.

5.3 $PM_{2.5}$ infiltrations under varying Q_{50} for all zones

The co-simulations also facilitate assessment of $PM_{2.5}$ infiltrations with varying Q_{50} settings. By aggregating all the zones across the four buildings (N=455), we can get a view of the impact of Q_{50} on infiltrated $PM_{2.5}$ over the heating season and for a year (**Table 9**). It can be noted that the average heating season concentrations of infiltrated $PM_{2.5}$ were 3.94 ± 0.98 $\mu g/m^3$ when Q_{50} = 3 $m^3/h/m^2$ (well-sealed envelope). While the Q_{50} was set at 13 $m^3/h/m^2$ (leaky envelope), the average heating season concentrations were 6.9 ± 1.14 $\mu g/m^3$, about 57% higher than Q_{50} = 3 $m^3/h/m^2$.

Table 9: Descriptive statistics of the infiltrated $PM_{2.5}$ by varying Q_{50} over the Heating Season and the (*Annual Average Concentrations*).

Q_{50} ($m^3/h/m^2$)	Number of Zones	Min-Max ($\mu g/m^3$)	Mean ($\mu g/m^3$)	Median ($\mu g/m^3$)	Standard Deviation	Variance
3	455	0.61-7.19 *(2.16-11.29)*	3.94 *(6.86)*	3.90 *(6.85)*	0.98 *(1.36)*	0.97 *(1.85)*
5	455	0.98-7.96 *(2.97-12.23)*	4.86 *(8.09)*	4.94 *(8.18)*	1.08 *(1.46)*	1.16 *(2.12)*
7	455	1.34-8.43 *(3.65-12.90)*	5.54 *(8.99)*	5.65 *(9.12)*	1.17 *(1.56)*	1.36 *(2.44)*
9	455	1.70-8.64 *(4.27-13.24)*	5.92 *(9.51)*	6.11 *(9.77)*	1.14 *(1.51)*	1.31 *(2.29)*
11	455	2.03-8.98 *(4.81-13.70)*	6.57 *(10.41)*	6.76 *(10.61)*	1.12 *(1.42)*	1.25 *(2.02)*
13	455	2.33-9.24 *(5.28-14.06)*	6.90 *(10.87)*	7.12 *(11.11)*	1.14 *(1.45)*	1.30 *(2.09)*

The outputs also show a clear relationship between the Q_{50} value and the infiltration air change rates ACH_{INF} during the heating season. As the Q_{50} value increased, the ACH_{INF} also increased, indicating a higher air exchange rate between indoor and outdoor environments. **Table 10** shows that the mean ACH_{INF} progressively increased from 0.38 h^{-1} for Q_{50} = 3 $m^3/h/m^2$ to 1.37 h^{-1} for Q_{50} = 13 $m^3/h/m^2$. This represents a substantial increase of approximately 260.5% in the ACH_{INF} over the heating season due to a leaky building envelope (**Figure 12**).

Table10: Descriptive statistics for the ACH_{INF} with varying Q_{50} over the heating season (Nov–April)

Q_{50} ($m^3/h/m^2$)	Number of Zones	Min-Max (h^{-1})	Mean (h^{-1})	Median (h^{-1})	Standard Deviation	Variance
3	455	0.06-1.57	0.38	0.32	0.23	0.05
5	455	0.11-2.22	0.60	0.50	0.37	0.14
7	455	0.16-2.97	0.84	0.72	0.51	0.26
9	455	0.20-3.63	0.97	0.81	0.57	0.32
11	455	0.24-4.32	1.17	0.97	0.72	0.52
13	455	0.28-5.02	1.37	1.14	0.84	0.71

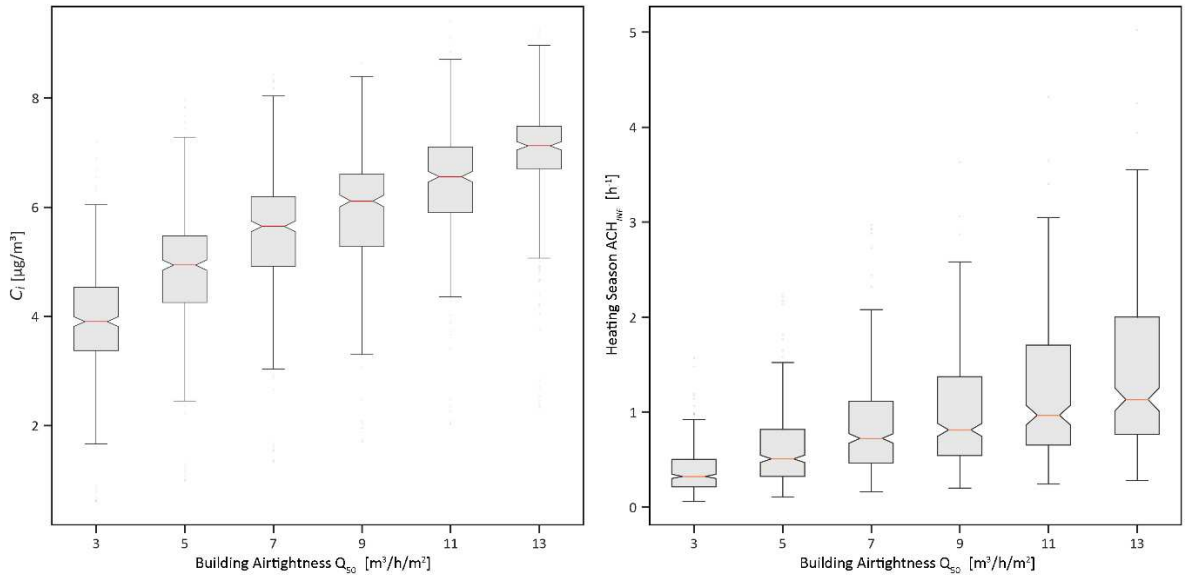

Figure 1: Box plots of the Heating Season Concentrations of Infiltrated $PM_{2.5}$ C_i and the ACH_{INF} stratified by the building envelope airtightness (Q_{50})

With reference to the WHO $PM_{2.5}$ recommendations (before and after 2021), **Figure 13** shows a cumulative distribution function plot of the annual concentrations of $PM_{2.5}$ with varying Q_{50} settings across all zones simulated (N=455). As the Q_{50} increased, there was a noticeable reduction in the percentage of zones exceeding the WHO recommended threshold (10 µg/m^3). For Q_{50} of 13 $m^3/h/m^2$, the percentage of exceedance was 82%, with a total of 373 zones exceeding 10 µg/m^3 guideline. A decrease in the Q_{50} to 11 resulted in a slightly lower but still significant percentage of exceedance of 77%, with 350 zones surpassing 10 µg/m^3. The trend of decreasing exceedance percentages continued as the Q_{50} value decreased further. For Q_{50} of 5, the percentage of exceedance was reduced to 4%, with only 25 zones exceeding the limit. The lowest percentage of exceedance was observed for the Q_{50} value of 3 (well-sealed), where only 1% of zones exceeded the WHO limit, with 5 zones surpassing 10 µg/m^3. On the other hand, the CDF result indicates the challenge of meeting the latest more stringent WHO recommendation of 5 µg/m^3 across the board, even with Q_{50} of 3 $m^3/h/m^2$ (well-sealed).

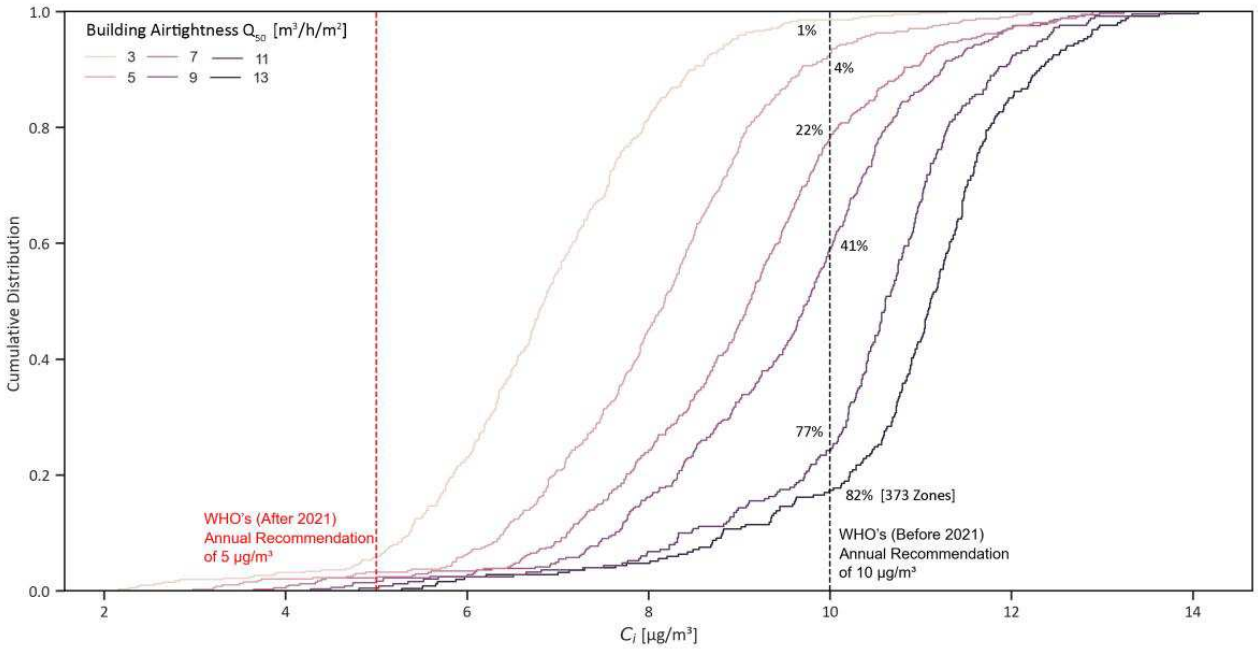

Figure 2: Cumulative distribution function (CDF) showing the percentage of zones with an annual average concentration of infiltrated $PM_{2.5}$ above the WHO guidelines of 10 µg/m^3 (before 2021) and 5 µg/m^3 (after 2021)

5.4 $PM_{2.5}$ indoor/outdoor (I/O) ratios

The indoor/outdoor (I/O) ratio is a metric used to compare the concentration of a specific air pollutant indoors to its concentration outdoors. Thus, $PM_{2.5}$ I/O ratio can be used to assess the disparity between indoor $PM_{2.5}$ concentrations and the corresponding outdoor concentrations and gauge indoor sources' strength within buildings. **Table 11** summarises the heating season and annual $PM_{2.5}$ I/O ratio when stratified by Q_{50}. It was found from the co-simulation results that the annual I/O ratio range between 0.26-1.03 for all zones, with an average of 0.66 ± 0.06 when Q_{50} = 3 m^3/h/m^2. This indicates a high spatial variability of infiltrated $PM_{2.5}$ concentrations within the same building as well as across different buildings sharing the same Q_{50}. This spatial disparity in infiltrated $PM_{2.5}$ observed here highlights the importance of implementing the model resolution of "individual zones" as the essential base unit in estimating population exposure to indoor air pollutants in HEI buildings.

Table 11: Descriptive statistics of $PM_{2.5}$ indoor/outdoor (I/O) with stratified Q_{50} over the Heating Season and the (*Annual Average*)

Q_{50} (m^3/h/m^2)	Number of Zones	Min-Max I/O	Mean I/O	Median I/O	Standard Deviation	Variance
3	455	0.04-0.42	0.23	0.23	0.06	<0.01
		(0.26-1.03)	*(0.66)*	*(0.66)*	*(0.11)*	*(0.01)*
5	455	0.06-0.47	0.29	0.29	0.06	<0.01
		(0.35-1.11)	*(0.76)*	*(0.50)*	*(0.12)*	*(0.01)*
7	455	0.08-0.49	0.33	0.33	0.07	<0.01
		(0.42-1.16)	*(0.83)*	*(0.84)*	*(0.13)*	*(0.02)*
9	455	0.10-0.51	0.35	0.36	0.07	<0.01
		(0.48-1.19)	*(0.88)*	*(0.81)*	*(0.12)*	*(0.02)*
11	455	0.12-0.53	0.39	0.40	0.07	<0.01

		(0.53-1.22)	*(0.95)*	*(0.97)*	*(0.11)*	*(0.01)*
13	455	0.14-0.54	0.41	0.42	0.07	<0.01
		(0.57-1.25)	*(0.99)*	*(1.01)*	*(0.11)*	*(0.01)*

We take a closer look into the relationship between indoor and outdoor $PM_{2.5}$ concentrations using the outputs from two zones in Building 3(RC), Zone (1) and Zone (2), both located on the first floor. The focal point here is the determination coefficient (R^2) values, which provide insights into the degree of correlation between indoor and outdoor $PM_{2.5}$ daily concentrations where the Q_{50} was 3 and 7 $m^3/h/m^2$ respectively (**Figure 14**). For Zone (1), with a Q_{50} of 7, the R^2 value between outdoor and indoor $PM_{2.5}$ concentrations was 0.89. This suggests that approximately 89% of the variation in indoor $PM_{2.5}$ concentrations can be attributed to changes in outdoor $PM_{2.5}$ levels, indicating a more robust correlation than the Q_{50} of 3 (R^2 = 0.85). Similarly, for Zone (2), with Q_{50} of 7, the R^2 value was 0.83, indicating a significant correlation between outdoor and indoor $PM_{2.5}$ when compared to Q_{50} of 3 (R^2 = 0.72).

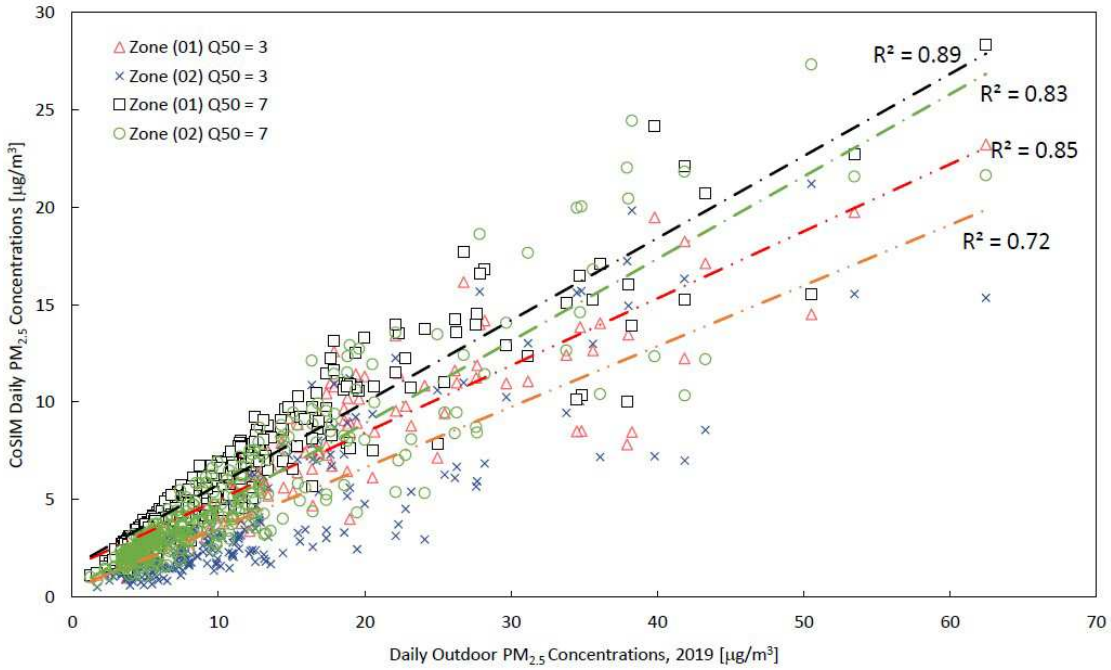

Figure 3: Scatter plots of daily outdoor $PM_{2.5}$ concentrations and daily infiltrated $PM_{2.5}$ in 2 different zones in Building 3 (RC) as an example, where Q_{50} = 3 and 7 $m^3/h/m^2$ respectively

Using the outputs from Building 4 (AT), the relationship between outdoor and indoor $PM_{2.5}$ concentrations was also analysed in two different zones, Zone (1) on the 3rd floor and Zone (2) on the 12th floor, to see the variations of indoor $PM_{2.5}$ on different floor levels of a tower block (**Figure 15**). It can be noticed that Zone (1) on the 3rd floor exhibited a strong correlation between outdoor and indoor $PM_{2.5}$ (R^2=0.95) with Q_{50} of 7. Similarly, Zone (2) on the 12th floor showed a moderately strong relationship (R^2=0.79), with the same Q_{50} (=7). While increasing the airtightness to Q_{50}=3, Zone (1) exhibited R^2=0.90. This indicates that although the relationship between outdoor and indoor $PM_{2.5}$ concentrations remains strong, the improvement in airtightness led to a slight reduction in R^2. Similarly, R^2 decreased to 0.66 in Zone (2), showing a weaker relationship between outdoor and indoor $PM_{2.5}$ after increased airtightness.

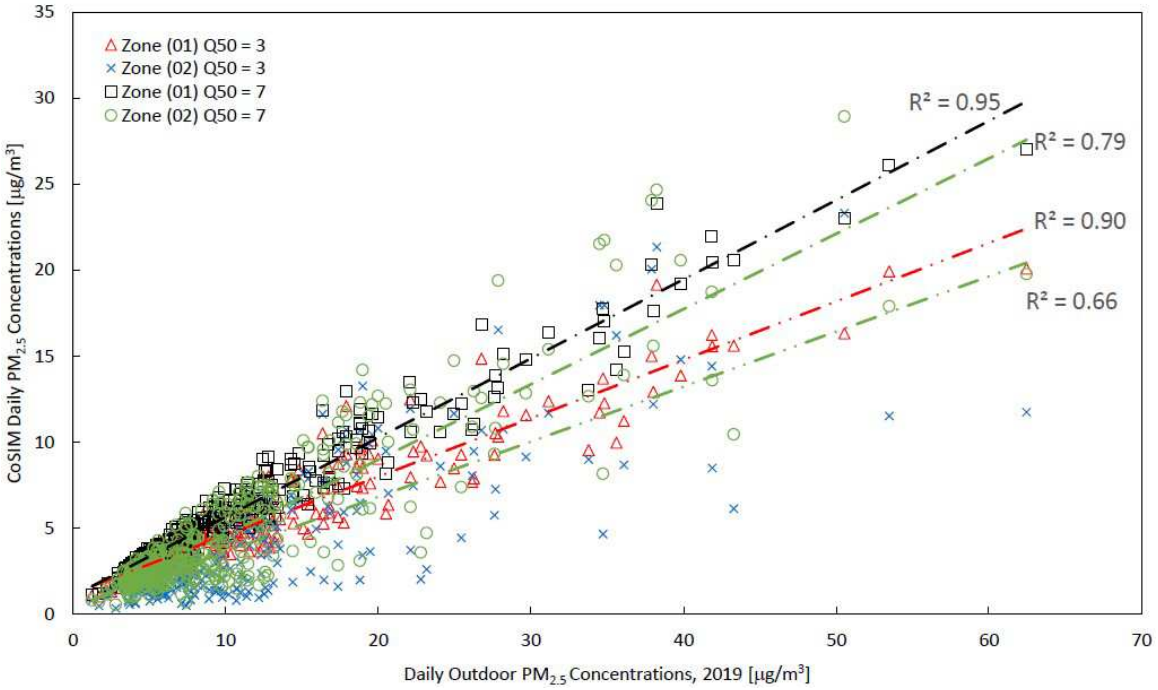

Figure 4: Scatter plots of daily outdoor $PM_{2.5}$ concentrations and daily infiltrated $PM_{2.5}$ in 2 different zones in Building 4 (AT) as an example, where Q_{50} = 3 and 7 $m^3/h/m^2$ respectively

6. Discussion

6.1 Data sources for IAQ modelling of HEI buildings

Previous studies on building stock indoor air quality (IAQ) and energy modelling have identified two key data requirements: data demand and data robustness (Abdalla & Peng, 2021). Data demand encompasses the scope, quantity, and type of input data necessary for accurate and consistent predictions (Sousa et al., 2017). While residential building stock studies often rely on national population and housing censuses for essential statistical information, collating a representative database for Higher Education Institution (HEI) building simulation pose challenges due to the absence of systematic survey data and their inherent heterogeneity in geometry, function, and use. Consequently, this study focused on selected buildings rather than statistical archetypes. While the Higher Education Statistics Agency (HESA) collects general HEI data, it lacks detailed building stock information, necessitating reliance on HEI Estates and Facilities Management (EFM) records for data on building characteristics, ventilation, and heating policies. However, challenges remain, including outdated records due to refurbishments and inconsistencies across buildings, requiring assumptions in model inputs. These issues highlight the need for HEI EFMs to develop comprehensive and consistent databases of building properties to enable accurate assessment and prediction of indoor air quality performance.

The deposition rate k=0.39 h^{-1} represents a spatial average across diverse room types. While furniture density and air velocity may cause localised variations, this value aligns with prior studies of non-domestic buildings. Using a simplified inverse proportionality method, preliminary tests with deposition rates of k=0.2 h^{-1} and k=0.6 h^{-1} revealed that a ±30% change in k resulted in a ±8–12% variation in annual $PM_{2.5}$ concentrations, with relative trends across Q_{50} scenarios remaining consistent. Future work should incorporate zone-specific deposition rates based on detailed surveys or CFD analysis.

Regarding window operation, the study modelled this according to prevailing building management policies and typical seasonal practices at the University of Sheffield. During the heating season (November–April), windows were assumed to be closed, reflecting university heating policy and efforts to conserve energy. Conversely, during the non-heating season (May–October), windows were assumed to be open to represent natural ventilation for cooling and fresh air. While this approach provided clear boundary conditions aligned with available operational data, it is acknowledged that this is a simplification. In practice, occupant behaviour, such as occasional window opening during the heating season, is influenced by individual comfort, air quality perception, and specific room use. However, due to the absence of comprehensive, zone-level data on actual window opening frequency, duration, and timing across the 2,729 zones and five buildings, it was not feasible to parameterise intermittent or probabilistic window opening in the current model. The chosen approach provides a conservative estimate of infiltration-driven $PM_{2.5}$ exposure during periods when infiltration is likely the dominant pathway for outdoor pollutants. This omission of detailed human factors in window operation is recognised as a limitation. Future studies should incorporate occupant surveys, sensor-based monitoring, or stochastic modelling of window operation to better capture the variability introduced by human factors and to simulate mixed-mode ventilation scenarios more realistically.

6.2 Necessity of a multi-zone air-thermal coupled simulation

Indoor air pollution can be estimated using building simulations when sufficient field measurements are unavailable, with single-zone mass balance models being the simplest approach, representing all indoor spaces as a single air volume (Jung et al., 2011). These models have been used to study outdoor $PM_{2.5}$ infiltrations (Fazli et al., 2021; Rosofsky et al., 2019), the dilution of indoor contaminants (Ng et al., 2021), and large-scale planning impacts (Abdalla & Peng, 2021. However, single-zone models lack the spatial resolution needed to capture IAQ-related health impacts due to building-specific variations. In contrast, multi-zone models, such as CONTAM, better reflect the compartmentalised nature of HEI buildings and allow for the evaluation of exposure and health impacts of IAQ interventions (Underhill et al., 2020).

The CONTAM-EnergyPlus coupling enables simultaneous thermal, airflow, and contaminant transport simulations, revealing key sensitivities, such as the influence of building envelope airtightness (Q_{50}) on infiltration airflow rates (ACH_{INF}) and indoor $PM_{2.5}$ levels. For instance, during the heating season, ACH values varied from 0.28 to 5.02 h^{-1} for buildings with Q_{50} = 13 $m^3/h/m^2$, with $PM_{2.5}$ concentrations ranging from 2.33 to 9.24 $\mu g/m^3$, with higher ACH correlating to higher infiltrations. This underscores the importance of carefully selecting envelope leakage rates in IAQ simulations, as they significantly influence airflow and $PM_{2.5}$ infiltrations. Given the limited data on envelope leakage in UK HEI buildings, accurate selection of these values remains a challenge for IAQ and airflow analysis.

While constant infiltration rates are often used in energy simulations, they fail to account for weather effects, necessitating more dynamic infiltration treatments. Multi-zone airflow models estimate pressure relationships between building zones, incorporating factors such as geometry, exposure, inter-zone leakage, and exhaust airflow, while thermal models focus on energy loads and system efficiency. Since thermal zoning alone may not sufficiently capture airflow dynamics, coupled IAQ-Thermal simulations offer a more robust approach for predicting indoor $PM_{2.5}$. As UK HEI heating policies regulate indoor temperature based on outdoor conditions, a coupled IAQ-Energy multi-

zone simulation approach is necessary to capture the dynamic interplay between temperature differences and $PM_{2.5}$ concentrations, making it a critical tool for analysing HEI buildings.

6.3 Spatiotemporal variations of $PM_{2.5}$ infiltrations

The coupled simulation of the selected HEI buildings revealed significant spatial variability in infiltrated $PM_{2.5}$ concentrations across different rooms and spaces within each building. Analysis of indoor $PM_{2.5}$ time-series data in Section 5.1 supported the need for high spatial resolution modelling, as individuals within the same building experience varying pollution levels due to daily activity patterns (Elliot et al., 2000). Disparities in exposure based on socio-economic groups (Ferguson et al. 2020) further emphasize the importance of studying indoor air quality across diverse building types. More recent research by Milando et al. (2022) examined the effects of building characteristics, HVAC systems, and model resolution on $PM_{2.5}$ exposures in Boston housing typologies, showing that finer room- or floor-level model resolution altered exposure estimates for indoor-sourced $PM_{2.5}$, though single-zone models sufficed for outdoor-sourced $PM_{2.5}$.

However, HEI buildings demand higher resolution due to their scale, geometry, and complex airflow networks, which differ markedly from residential settings. Limited research has focused on non-domestic building stocks, with notable exceptions like the UK Classrooms Archetype Stock Model (Schwartz et al., 2021), which used thermal zones rather than detailed airflow networks, neglecting factors like ambient weather conditions and spatial variability in pollution. This study addresses this gap by developing a high-resolution IAQ-thermal model to capture spatial variability in infiltrated $PM_{2.5}$ concentrations during the heating season. To quantify this variability and determine the key factors influencing $PM_{2.5}$ infiltrations, a further comprehensive sensitivity analysis is required. While Figure 8 highlights significant differences in $PM_{2.5}$ concentrations among rooms with varying orientations within the same building, the current study primarily focused on developing a data-centric approach to assess and quantify the potential effects of building airtightness (Q_{50}) on $PM_{2.5}$ infiltration. The model did account for the effects of local wind conditions on each side of the buildings by estimating wind pressure profiles using wind pressure coefficient relationships, which are a function of the block aspect ratio and terrain constants. However, a specific quantitative correlation analysis between room orientation, wind speed/direction, and $PM_{2.5}$ concentrations (e.g., involving wind rose diagrams) was not within the scope of this study. Further detailed analysis, including such a correlation, represents a promising avenue for future comprehensive sensitivity analysis to fully determine the key environmental and building characteristics influencing $PM_{2.5}$ infiltrations.

6.4 Simulated average $PM_{2.5}$ I/O ratios

The results from the three scenarios (baseline Q_{50}, Q_{50} = 7 $m^3/h/m^2$, and Q_{50} = 3 $m^3/h/m^2$) provide insights into the average $PM_{2.5}$ I/O ratios during heating and non-heating seasons. The I/O ratio, representing the ratio of indoor to outdoor $PM_{2.5}$ concentrations, highlights the influence of infiltration rates (ACH_{INF}) and outdoor $PM_{2.5}$ levels on indoor air quality. During the heating season (November–April), when infiltration is the primary airflow source, the $PM_{2.5}$ I/O ratio for the Q_{50} = 3 $m^3/h/m^2$ scenario (0.23 ± 0.06) is significantly lower than the baseline Q_{50} scenario (0.37 ± 0.06), indicating that reduced infiltration rates decrease outdoor $PM_{2.5}$ infiltrations (**Figure 16**). This is supported by lower average indoor $PM_{2.5}$ concentrations in the Q_{50} = 3 $m^3/h/m^2$ scenario (3.94 ± 0.98 $\mu g/m^3$) compared to the baseline Q_{50} scenario (6.30 ± 1.07 $\mu g/m^3$) (**Figure 17**). Conversely, during the non-heating season (May–October), when natural ventilation dominates (windows opened), $PM_{2.5}$ I/O ratios remain stable across scenarios, and indoor $PM_{2.5}$ concentrations are

consistently lower than those during the HEI heating season. This reflects greater indoor-outdoor interactions while natural ventilation increases air change rates during May–October.

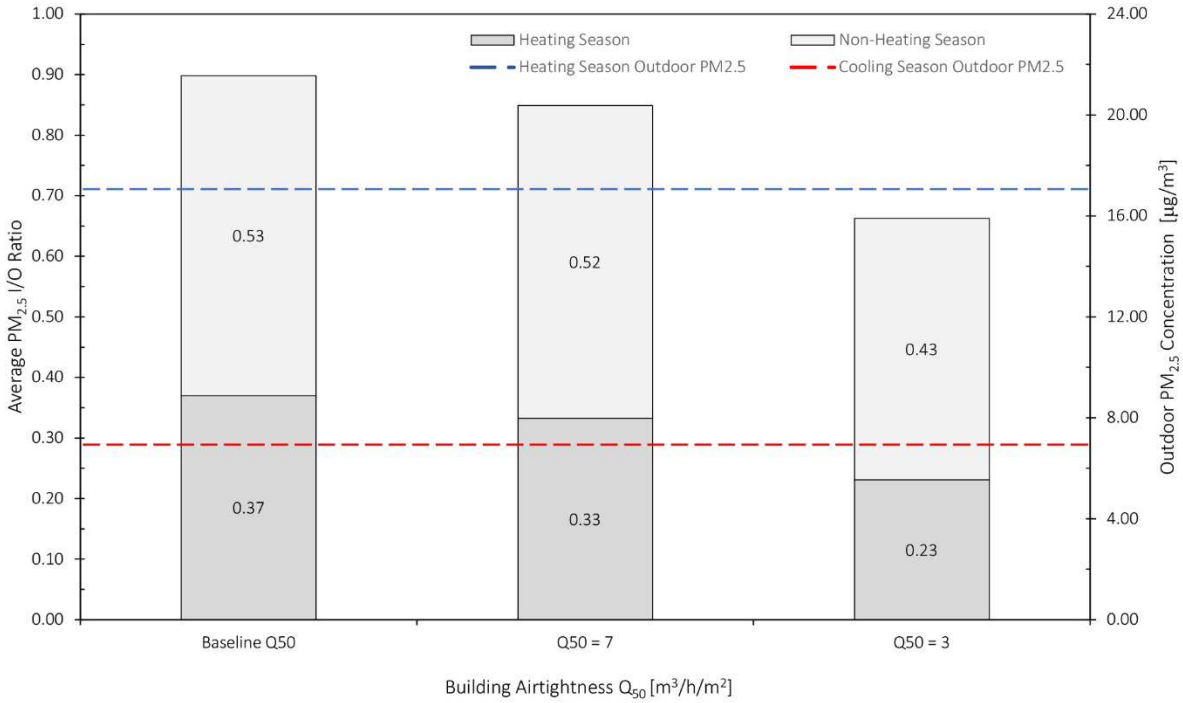

Figure 16: Average seasonal $PM_{2.5}$ I/O ratios under three scenarios of Q_{50}, and seasonal variation in outdoor $PM_{2.5}$ concentrations (µg/m3)

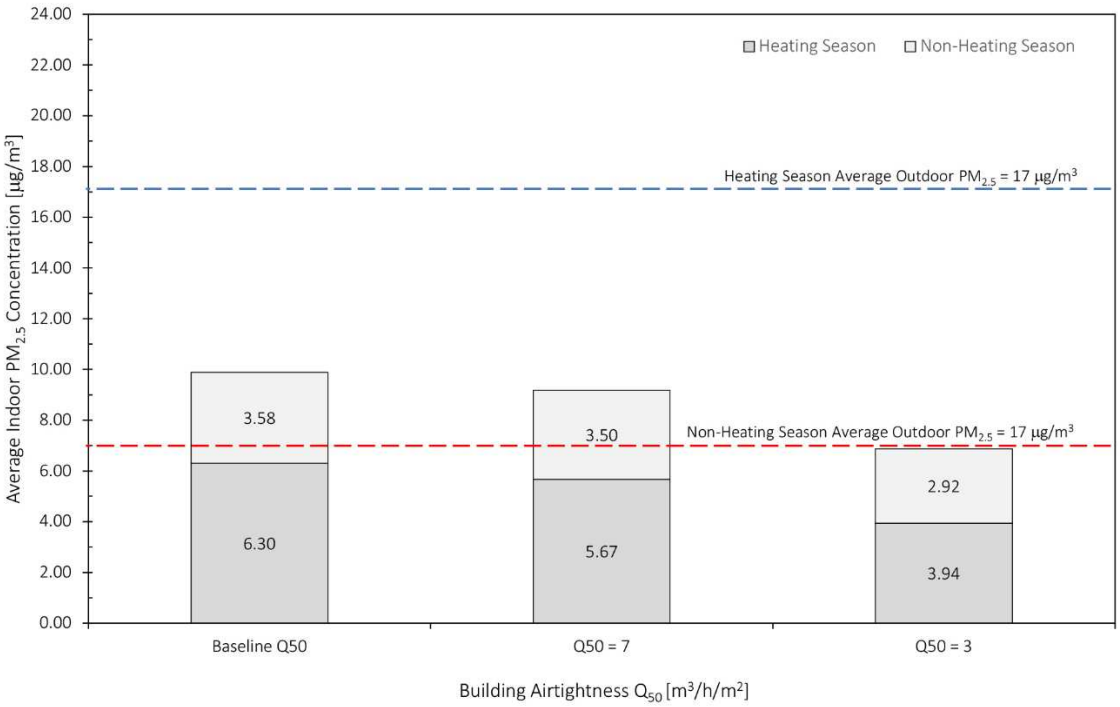

Figure 17: Average seasonal indoor $PM_{2.5}$ concentrations under three Q_{50} scenarios, and seasonal variation in outdoor $PM_{2.5}$ concentrations (µg/m^3)

The higher $PM_{2.5}$ I/O ratios and indoor $PM_{2.5}$ concentrations during the heating season highlight its critical role in IAQ management. The increased infiltration of outdoor pollutants leads to elevated indoor $PM_{2.5}$ levels, making it essential to prioritize mitigation strategies such as reducing infiltration rates and lowering outdoor $PM_{2.5}$ concentrations. Potential measures include enhancing building envelope insulation, implementing air filtration systems, and minimising air leakage. Furthermore, reducing outdoor $PM_{2.5}$ emissions is crucial to limiting the impact of external pollution on indoor environments. In comparison with related studies on $PM_{2.5}$ I/O ratios, no observational studies of $PM_{2.5}$ I/O ratios specific to HEI buildings are available. Broader studies reported that indoor sources can significantly contribute to indoor $PM_{2.5}$ in residential settings with $PM_{2.5}$ I/O ratios close to or exceeding one (Jones et al., 2013; Lai et al., 2006). A study conducted in European countries found the $PM_{2.5}$ I/O ratios ranging from 0.30 to 0.70 (Hänninen et al., 2011), while a comprehensive review of large-scale studies of homes in different cities suggested a range between 0.30 and 0.82 (Chen and Zhao, 2011). A long-term IAQ monitoring study of a naturally ventilated office located in Keynsham, England, reported $PM_{2.5}$ I/O ratio of 0.69 and the highest median indoor concentration of 3.7 $\mu g/m^3$, despite lower ambient concentrations of 5.4 $\mu g/m^3$ (Stamp et al., 2020). The simulated $PM_{2.5}$ I/O ratios of this study show a range of 0.42 to 1.16 (Q_{50} = 7 $m^3/h/m^2$), and 0.26 to 1.03 (Q_{50} = 3 $m^3/h/m^2$), indicating some alignment with the previous findings.

6.5 Validation of the co-simulation

CONTAM and EnergyPlus as building simulation tools have been widely used in research for over thirty years. Several validation studies have been conducted on different building types, locations and pollutants (e.g., Emmerich & Hirnikel, 2001; Ng et al., 2012; Underhill et al., 2018). In this study, a field measurement campaign intended for validating the co-simulation results in this study was not implemented due to the nationwide COVID-19 lockdowns enforced at the time. If there were no pandemic during 2020-21, our validation of the co-simulation would have been carried out according to the Standard Guide for Statistical Evaluation of Indoor Air Quality Models (ASTM D5157-19). According to the standard guide, the following measures can be used to determine if model predictions agree with observations (field measurements). If there were no pandemic during 2020-21, the following measures would have been applied to determine if the co-simulations agreed with the fields measurements:

- Predictions and measurements should have a correlation coefficient of 0.9 or greater.
- The regression line between predictions and measurements should have a slope between 0.75 and 1.25 and an intercept of less than 25% of the average concentration.
- The normalised mean square error (NMSE) is less than 0.25 and can be calculated as follows:

$$NMSE = \sum_{i=1}^{N} \frac{(C_{pi} - C_{oi})^2}{(C_o C_p)} \qquad \textbf{(Eq. 8)}$$

  Where N is the number of observations (measurements) in the datasets, Cp is the predicted concentration and Co is the observed concentration.

However, an indirect validation was attempted by accessing the field measurements acquired by a separate study of Building 4 (AT), where indoor environmental data (temperature, humidity, and CO_2) of an office on the 9th floor was collected in the summer of 2022. The measurements were taken on a 5-min time-step between 11:00 AM on 11/05/2022 and 11:00 AM on 17/05/2022, resulting in a sample size of 1,720 data points. The sensor and data logger (HOBO UX100-003) were placed in the middle of the room and were 1 meter above floor level (**Table 12**).

Table 12: Results of the validation (Indoor air temperatures, Floor 9, Arts Tower)

Properties of the room used for the indirect validation of the co-simulation (indoor temperature only)					
Date and Time of Measurements		11/05/2022 (11:00 AM) – 17/05/2022 (11:00 AM)			
Location		Room 9.02 on the 9th Floor of Building 4 (AT)			
Orientation	North	Number of Occupants at the Time of Measurement	1		
Room Area	46 m^2	Heating Policy	Off		
Q_{50}	10 $m^3/h/m^2$	External Wall	Double Glazed Curtain Wall U-Value 2.2 $W/m^2.K$		
		Windows	Closed		
		Results			
	Number of Samples	Average Indoor Temperature	Standard Deviation	Correlation Coefficient	NMSE
Co-Simulation Results	1,720	22.34 °C	1.029	0.76	0.48
Field Measurements	1,720	22.47 °C	0.986		

Figure 18 shows the overall correlation coefficient of 0.76 with an NMSE of 0.48, indicating some agreement between the simulated results and field measurements for indoor temperature. The difference between the average values was only 0.07 °C, so these values were considered reasonable for indoor air temperature validation. However, they were lower than the standard values specified in the ASTM guide.

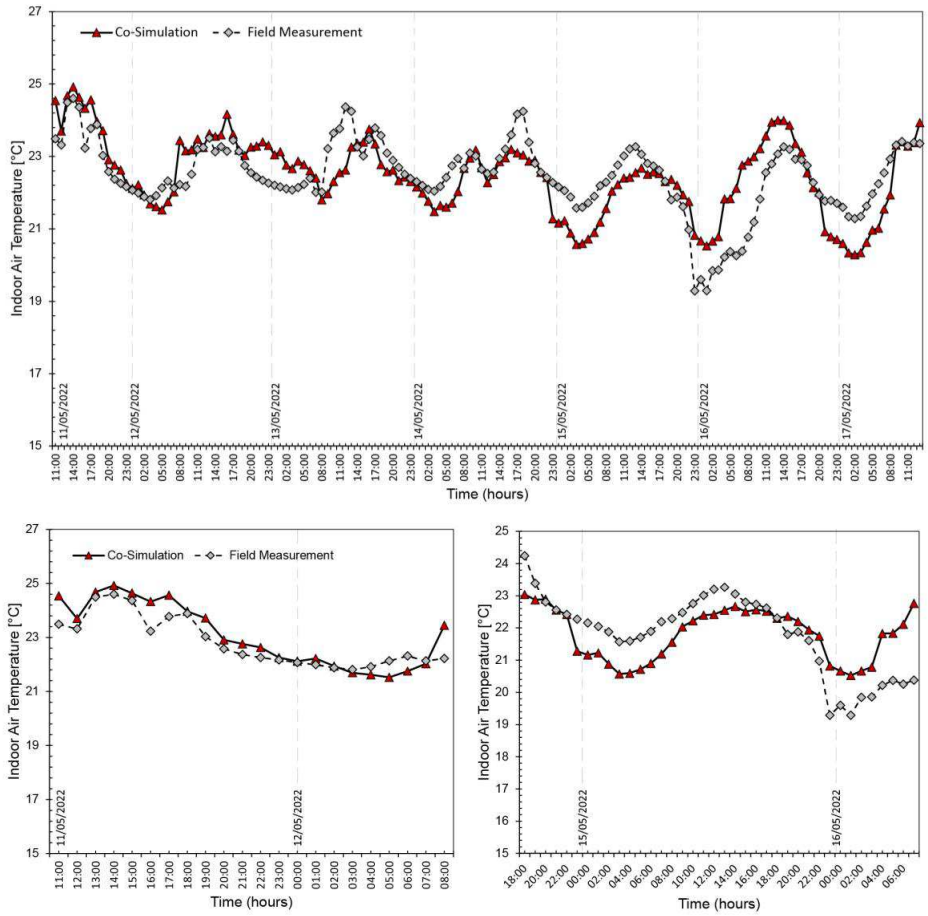

Figure 18: Simulated and observed indoor air temperature (°C). Dates 11-17/05/2022, Location: North-facing office on the 9th Floor of Building 4 (AT)

7. Conclusion

The study aims to develop a data-centric approach to rapidly assessing and quantifying potential effects of building airtightness (Q_{50}) on seasonal and annual average fine particulate matter ($PM_{2.5}$) infiltration from outdoor sources in the HEI context. The goal was achieved by employing the building physics implemented in the air-thermal co-simulation framework using CONTAM and EnergyPlus. The primary data sources for facilitating the co-simulation study are provided by the HEI's Estates and Facilities Management (EFM). The current paucity of HEI environmental and building information required for the influential variables involved in the co-simulation can be improved for future studies. For instance, we show that the data of building envelope airtightness level (Q_{50}) of HEI buildings is mostly scarce and the absence of this data becomes a primary source of uncertainty in building simulation.

With assumed baseline Q_{50} values (3-13 $m^3/h/m^2$) of the buildings selected for the study, the co-simulation results show distinct annual average concentrations of indoor $PM_{2.5}$ across the buildings studied. Building 1 (BH) exhibits a concentration range of 8.11-14.06 µg/m³, while Building 2 (ADC) has a slightly lower range of 5.28-12.61 µg/m³. Building 4 (AT) and Building 3 (RC) are in the ranges of 5.59-13.82 µg/m³ and 7.71-13.15 µg/m³, respectively. The variability in $PM_{2.5}$ concentrations within each building is evident, as indicated by the standard deviation and variance values. Accounting for the distribution of $PM_{2.5}$ concentrations at the zoom/zone level, all buildings exhibit different levels of spatiotemporal variability.

Analysing the simulation outputs of infiltrated $PM_{2.5}$ over the heating season and for a year provides insights into the relationships between Q_{50}, infiltration air change rates (ACH_{INF}), estimated indoor $PM_{2.5}$ concentrations, and the percentage of zones exceeding the WHO recommendations. The study found that a significant proportion of zones within each building exceeds the WHO recommended annual average concentration of $PM_{2.5}$ (10 µg/m³, 2005 guideline), raising concerns about IAQ and its potential health implications for building users. The substantial increase in ACH_{INF}, approximately 260.5%, over the heating season due to high Q_{50} (a leaky building envelope) underscores the significance of airtightness improvements in controlling air exchange and reducing air pollutant infiltration. In the low Q_{50} (=3) scenario (a well-sealed envelope), we found that a significant proportion (approaching 88%) of the zones exceeding the WHO $PM_{2.5}$ 2021 guideline (5 µg/m³) was present across the buildings, indicating the limit of what low Q_{50} may be able to achieve if outdoor ambient air pollution levels stay above certain thresholds. Indoor $PM_{2.5}$ exceedances are driven by both elevated outdoor concentrations and building airtightness. While reducing Q_{50} lowers infiltration, achieving WHO compliance in high-pollution regions requires parallel strategies to reduce ambient PM2.5 (e.g., clean air zones, traffic reduction). Further research is required to identify such thresholds to inform citywide evidence-based air quality policies and regulations such as the necessity of clean air zone.

References

Abbaspour, A., Bahadori-Jahromi, A., Amirkhani, S., Janbey, A., Godfrey, P. B., Tahayori, H., & Piechowicz, J. (2023). Multi-Zonal Analysis of Indoor Air Quality in a Higher Educational Building in the UK. Sustainability, 15(16), 12118. https://doi.org/10.3390/su151612118

Abdalla, T., & Peng, C. (2021). Evaluation of housing stock indoor air quality models: A review of data requirements and model performance. Journal of Building Engineering, 43(May), 102846. https://doi.org/10.1016/j.jobe.2021.102846

Afroz, R., Guo, X., Cheng, C.-W., Delorme, A., Duruisseau-Kuntz, R., & Zhao, R. (2023). Investigation of indoor air quality in university residences using low-cost sensors. Environnemental Science : Atmospheres, 3(2), 347–362. https://doi.org/10.1039/D2EA00149G

Apte, J. S., Brauer, M., Cohen, A. J., Ezzati, M., & Pope, C. A. (2018). Ambient $PM_{2.5}$ Reduces Global and Regional Life Expectancy. Environmental Science and Technology Letters, 5(9), 546–551. https://doi.org/10.1021/acs.estlett.8b00360

Arup. (2012). University of Sheffield Energy Strategy. May 2012.

ASTM (2019). ASTM D5157-19, Standard Guide for Statistical Evaluation of Indoor Air Quality Models. West Conshohocken, PA: ASTM International. https://doi.org/10.1520/D5157-19

Axley, J. W. (1987). Indoor Air Quality Modeling Phase II Report. In NBSIR 87-3661. National Bureau of Standards (U.S.).

Axley, J. W. (1988). Progress Toward a General Analytical Method for Predicting Indoor Air Pollution in Buildings, Indoor Air Quality Modelling Phase III Report. In NBSIR 88-3814. National Bureau of Standards (U.S.).

Axley, J. W. (2007). Multizone airflow modeling in buildings: History and theory. HVAC and R Research, 13(6), 907–928. https://doi.org/10.1080/10789669.2007.10391462

Blochwitz, T., Otter, M., Arnold, M., Bausch, C., Clauss, C., Elmqvist, H., Junghanns, A., Mauss, J., Monteiro, M., Neidhold, T., Neumerkel, D., Olsson, H., Peetz, J.-V., & Wolf, S. (2011). The Functional Mockup Interface for Tool independent Exchange of Simulation Models. Proceedings from the 8th International Modelica Conference, Technical Univeristy, Dresden, Germany, 63, 105–114. https://doi.org/10.3384/ecp11063105

Chen, C. & Zhao, B. (2011). Review of relationship between indoor and outdoor particles: I/O ratio, infiltration factor and penetration factor, Atmospheric Environment, 45(2), 2011, 275-288. https://doi.org/10.1016/j.atmosenv.2010.09.048

Chen, J., Braun, D., Christidis, T., Cork, M., Rodopoulou, S., Samoli, E., Stafoggia, M., Wolf, K., Wu, X., Yuchi, W., Andersen, Z., Atkinson, R., Bauwelinck, M., De Hoogh, K., Janssen, N., Katsouyanni, K., Klompmaker, J., Kristoffersen, D., Lim, Y., Oftedal, B., Strak, M., Vienneau, D., Zhang, J., Burnett, R., Hoek, G., Dominici, F., Brauer, M., & Brunekreef, B. (2023). Long-Term Exposure to Low-Level $PM_{2.5}$ and Mortality: Investigation of Heterogeneity by Harmonizing Analyses in Large Cohort Studies in Canada, United States, and Europe. Environmental Health Perspectives, 131. https://doi.org/10.1289/EHP12141

CIBSE (2005). Natural ventilation in non-domestic buildings: CIBSE Application Manual AM10:1997. 99.

CIBSE (2018). Environmental design CIBSE Guide A. In The Chartered Institution of Building Services Engineers, London. (Issue June).

CIBSE (2022). CIBSE TM23 Testing Buildings for Air Leakage.

Coleman, J. R., & Meggers, F. (2018). Sensing of indoor air quality—characterization of spatial and temporal pollutant evolution through distributed sensing. Frontiers in Built Environment, 4 (August), 1–12. https://doi.org/10.3389/fbuil.2018.00028

Conte, S. D., & de Boor, C. (1972). Elementary Numerical Analysis: An Algorithmic Approach.

Cserbik, D., Chen, J. C., McConnell, R., Berhane, K., Sowell, E. R., Schwartz, J., Hackman, D. A., Kan, E., Fan, C. C., & Herting, M. M. (2020). Fine particulate matter exposure during childhood relates to

hemispheric-specific differences in brain structure. Environment International, 143(December 2019), 105933. https://doi.org/10.1016/j.envint.2020.105933

Dols, W. S., & Polidoro, B. J. (2015). CONTAM User Guide and Program Documentation Version 3.2. Tech. rept. NIST.

Dols, W. S., Emmerich, S. J., & Polidoro, B. J. (2016). Coupling the multizone airflow and contaminant transport software CONTAM with EnergyPlus using co-simulation. Building Simulation, 9(4), 469–479. https://doi.org/10.1007/s12273-016-0279-2

Dols, W. S., & Polidoro, B. J. (2020). CONTAM User Guide and Program Documentation - Version 3.4 (NIST Technical Note 1887).

Dols, S., Milando, C., Ng, L., Emmerich, S., & Teo, J. (2021). On the Benefits of Whole-building IAQ, Ventilation, Infiltration, and Energy Analysis Using Co-simulation between CONTAM and EnergyPlus. Journal of Physics: Conference Series, 2069. https://doi.org/10.1088/1742-6596/2069/1/012183.

ECA. (2003). European Collaborative Action "Urban air, Indoor Environment and Human Exposure." Ventilation, Good Indoor Air Quality and Rational Use of Energy. Report No 23, EUR 20741 EN. Luxembourg: Office for Official Publications of the European Communities, 1–96.

Elliot, P., Wakefield, J. C., Best, N. G., & Briggs, D. J. (2000). Spatial epidemiology: methods and applications. Oxford University Press.

Emmerich, S. J., & Hirnikel, D. (2001). Validation of multizone IAQ modeling of residential- scale buildings: A review. ECAASHRAE Transactions, 107 PART 2(January 2001), 619–628.

Emmerich, S. J., Ng, L. C., & Dols, W. S. (2019). Simulation analysis of potential energy savings from air sealing retrofits of U.S. Commercial buildings. ASTM Special Technical Publication, STP 1615, 61–70. https://doi.org/10.1520/STP161520180021

Erlandson, G., Magzamen, S., Carter, E., Sharp, J. L., Reynolds, S. J., & Schaeffer, J. W. (2019). Characterization of Indoor Air Quality on a College Campus: A Pilot Study. International Journal of Environmental Research and Public Health, 16(15), 2721. https://doi.org/10.3390/ijerph16152721

Fazli, T., Dong, X., Fu, J. S., & Stephens, B. (2021). Predicting U.S. Residential Building Energy Use and Indoor Pollutant Exposures in the Mid-21st Century. Environmental Science & Technology, 55(5), 3219–3228. https://doi.org/10.1021/acs.est.0c06308

Feng, S., Gao, D., Liao, F., Zhou, F., & Wang, X. (2016). The health effects of ambient $PM_{2.5}$ and potential mechanisms. Ecotoxicology and environmental safety, 128, 67-74. https://doi.org/10.1016/j.ecoenv.2016.01.030.

Ferguson, L., Taylor, J., Davies, M., Shrubsole, C., Symonds, P., & Dimitroulopoulou, S. (2020). Exposure to indoor air pollution across socio-economic groups in high-income countries: A scoping review of the literature and a modelling methodology. Environment International, 143, 105748. https://doi.org/10.1016/j.envint.2020.105748

Feustel, H. E. (1999). COMIS-an international multizone air-flow and contaminant transport model. Energy and Buildings, 30(1), 3–18. https://doi.org/10.1016/S0378-7788(98)00043-7

Fine, J., & Touchie, M. (2021). Evaluating ventilation system retrofits for high-rise residential buildings using a CONTAM model. Building and Environment, 205, 108292. https://doi.org/10.1016/J.BUILDENV.2021.108292.

García-Tobar, J. (2019). Weather-dependent modelling of the indoor radon concentration in two dwellings using CONTAM. Indoor and Built Environment, 28(10), 1341–1349. https://doi.org/10.1177/1420326X19841119

Gillian, E. S., Bawa, Z., Macklin, Y., Morbey, R., Dobney, A., Vardoulakis, S., Elliot, A. J. (2015). Using real-time syndromic surveillance systems to help explore the acute impact of the air pollution incident of March/April 2014 in England, Environmental Research, 136, 500-504, https://doi.org/10.1016/j.envres.2014.09.028.

Haghighat, F. (1989). Air infiltration and indoor air quality models — a review. International Journal of Ambient Energy, 10(3), 115–122. https://doi.org/10.1080/01430750.1989.9675130

Haghighat, F., & Megri, A. (1996). A Comprehensive Validation of Two Airflow Models — COMIS and CONTAM. Indoor Air, 6, 278-288. https://doi.org/10.1111/J.1600-0668.1996.00007.X.

Hänninen, O., Hoek, G., Mallone, S., Chellini, E., Katsouyanni, K., Gariazzo, C., Cattani, G., Marconi, A., Molnár, P., Bellander, T., & Jantunen, M. (2011). Seasonal patterns of outdoor PM infiltration into indoor environments: review and meta-analysis of available studies from different climatological zones in Europe. Air Quality, Atmosphere & Health, 4, 221-233. https://doi.org/10.1007/S11869-010-0076-5.

Hensen, J., & Lamberts, R. (2011). Building Performance Simulation for Design and Operation. London, New York, Spon Press, 2011.

Jones, B., Das, P., Chalabi, Z., Davies, M., Hamilton, I., Lowe, R., Milner, J., Ridley, I., Shrubsole, C., & Wilkinson, P. (2013). The effect of party wall permeability on estimations of infiltration from air leakage. International Journal of Ventilation, 12(1), 17–29. https://doi.org/10.1080/14733315.2013.11683999

Jones, B., Phillips, G., O'Leary, C., Molina, C., & Hall, I. (2018). Diagnostic barriers to using $PM_{2.5}$ concentrations as metrics of indoor air quality. Paper presented at the Smart Ventilation for Buildings Conference, July 2018.

Jung, K. H., Bernabé, K., Moors, K., Yan, B., Chillrud, S. N., Whyatt, R., Camann, D., Kinney, P. L., Perera, F. P., & Miller, R. L. (2011). Effects of Floor Level and Building Type on Residential Levels of Outdoor and Indoor Polycyclic Aromatic Hydrocarbons, Black Carbon, and Particulate Matter in New York City. Atmosphere, 2(2), 96–109. https://doi.org/10.3390/atmos2020096

Klepeis, N. E., Nelson, W. C., Ott, W. R., Robinson, J. P., Tsang, A. M., Switzer, P., Behar, J. V., Hern, S. C., & Engelmann, W. H. (2001). The National Human Activity Pattern Survey (NHAPS): A resource for assessing exposure to environmental pollutants. Journal of Exposure Analysis and Environmental Epidemiology, 11(3), 231–252. https://doi.org/10.1038/sj.jea.7500165

Lai, H.K., Bayer-Oglesby, L., Colvile, R., Gotschi, T., Jantunen, M.J., Kunzli, N., Kulinskaya, E., Schweizer, C., Nieuwenhuijsen, M.J., (2006). Determinants of indoor air concentrations of $PM_{2.5}$, black smoke and NO2 in six European cities (EXPOLIS study). Atmospheric Environment 40, 1299-1313. https://doi.org/10.1016/j.atmosenv.2005.10.030

Lama, S., Fu, C., & Lee, A. (2022). Indoor Air Quality (IAQ) Evaluation of Higher Education Learning Environments. Journal of Smart Buildings and Construction Technology, 4(1), 1–14. https://doi.org/10.30564/jsbct.v4i1.4042

McDowell, T. P., Emmerich, S., Thornton, J. W., & Walton, G. (2003). Integration of airflow and energy simulation using CONTAM and TRNSYS. ASHRAE Transactions, 109 PART 2(March), 757–770. https://doi.org/10.1107/S1600536812032953

Megri, A. C., & Haghighat, F. (2007). Zonal modeling for simulating indoor environment of buildings: Review, recent developments, and applications. HVAC and R Research, 13(6), 887–905. https://doi.org/10.1080/10789669.2007.10391461

Milando, C. W., Carnes, F., Vermeer, K., Levy, J. I., & Fabian, M. P. (2022). Sensitivity of modeled residential fine particulate matter exposure to select building and source characteristics: A case study using public data in Boston, MA. Science of the Total Environment, 840(June), 156625. https://doi.org/10.1016/j.scitotenv.2022.156625

Miller, S. L., & Nazaroff, W. W. (2001). Environmental tobacco smoke particles in multizone indoor environments. Atmospheric Environment, 35(12), 2053–2067. https://doi.org/10.1016/S1352-2310(00)00506-9

Nazaroff, W. W., & Cass, G. R. (1987). Particle deposition from a natural convection flow onto a vertical isothermal flat plate, Journal of Aerosol Science, 18(4), 445-455. https://doi.org/10.1016/0021-8502(87)90042-5.

Nazaroff, W. W. (2004). Indoor particle dynamics. Indoor Air, Supplement, 14(SUPPL. 7), 175–183. https://doi.org/10.1111/j.1600-0668.2004.00286.x

Ng, L. C., Persily, A. K., & Emmerich, S. J. (2012). NIST Technical Note 1734 Airflow and Indoor Air Quality Models of DOE Reference Commercial Buildings. October.

Ng, L. C., Poppendieck, D., Polidoro, B., Dols, W. S., Emmerich, S., & Persily, A. (2021). Single-Zone Simulations Using FaTIMA for Reducing Aerosol Exposure in Educational Spaces. National Institute of Standards and Technology Technical Note 2150, 79. https://nvlpubs.nist.gov/nistpubs/TechnicalNotes/NIST.TN.2150.pdf%0Ahttps://doi.org/10.6028/NIST.TN.2150

O'Leary, C., de Kluizenaar, Y., Jacobs, P., Borsboom, W., Hall, I., & Jones, B. (2019). Investigating measurements of fine particle (PM 2.5) emissions from the cooking of meals and mitigating exposure using a cooker hood. Indoor Air, 29(3), 423–438. https://doi.org/10.1111/ina.12542

Panagopoulos, I. K., Karayannis, A. N., Kassomenos, P., & Aravossis, K. (2011). A CFD simulation study of VOC and formaldehyde indoor air pollution dispersion in an apartment as part of an indoor pollution management plan. Aerosol and Air Quality Research, 11(6), 758–762. https://doi.org/10.4209/aaqr.2010.11.0092

Persily, A. & Ivy, E. (2001), Input data for multizone airflow and IAQ analysis. National Institute of Standards and Technology, Gaithersburg, MD, [online], https://doi.org/10.6028/NIST.IR.6585 (Accessed March 1, 2025)

Rosofsky, A., Levy, J. I., Breen, M. S., Zanobetti, A., & Fabian, M. P. (2019). The impact of air exchange rate on ambient air pollution exposure and inequalities across all residential parcels in Massachusetts. Journal of Exposure Science & Environmental Epidemiology, 29(4), 520–530. https://doi.org/10.1038/s41370-018-0068-3

Schwartz, Y., Korolija, I., Symonds, P., Godoy-Shimizu, D., Dong, J., Hong, S. M., Mavrogianni, A., Grassie, D., & Mumovic, D. (2021). Indoor Air Quality and Overheating in UK Classrooms – an Archetype Stock Modelling Approach. Journal of Physics: Conference Series, 2069(1), 012175. https://doi.org/10.1088/1742-6596/2069/1/012175

Schweizer, C., Edwards, R. D., Bayer-Oglesby, L., Gauderman, W. J., Ilacqua, V., Juhani Jantunen, M., Lai, H. K., Nieuwenhuijsen, M., & Künzli, N. (2007). Indoor time- microenvironment-activity patterns in seven regions of Europe. Journal of Exposure Science and Environmental Epidemiology, 17(2), 170–181. https://doi.org/10.1038/sj.jes.7500490

Sherman, M. H., & Dickerhoff, D. (1998). Air-tightness of US dwellings. ASHRAE Transactions, American Society of Heating Refrigerating and Air Conditioning Engineers (ASHRAE), 104, 1359–1367.

Shimada, M., Okuyama, K., Okazaki, S., Asai, T., Matsukura, M., & Ishizu, Y. (1996). Numerical Simulation and Experiment on the Transport of Fine Particles in a Ventilated Room. Aerosol Science and Technology, 25(3), 242–255. https://doi.org/10.1080/02786829608965394

Smith, J. D., Mitsakou, C., Kitwiroon, N., Barratt, B. M., Walton, H. A., Taylor, J. G., Anderson, H. R., Kelly, F. J., & Beevers, S. D. (2016). London Hybrid Exposure Model: Improving Human Exposure Estimates to NO2 and $PM_{2.5}$ in an Urban Setting. Environmental Science & Technology, 50(21), 11760–11768. https://doi.org/10.1021/acs.est.6b01817

Sousa, G., Jones, B. M., Mirzaei, P. A., & Robinson, D. (2017). A review and critique of UK housing stock energy models, modelling approaches and data sources. Energy and Buildings, 151, 66–80. https://doi.org/10.1016/j.enbuild.2017.06.043

Stamp, S., Burman, E., Shrubsole, C., Chatzidiakou, L., Mumovic, D., & Davies, M. (2020). Long-term, continuous air quality monitoring in a cross-sectional study of three UK non-domestic buildings. Building and Environment, 180, 107071. https://doi.org/10.1016/j.buildenv.2020.107071.

Swami, M., & Chandra, S. (1987). Procedures for Calculating Natural Ventilation Airflow Rates in Buildings. Final report, FSEC-CR-163-8, Florida Solar Energy Center, Cape Canaveral, FL, 1–113.

Tabares-velasco, P. C. (2013). Time Step Considerations When Simulating Dynamic Behavior of High-Performance Homes. Thermal Performance of Exterior Envelopes of Whole Buildings XII, ASHRAE, 10.

Taylor, J., Shrubsole, C., Davies, M., Biddulph, P., Das, P., Hamilton, I., Vardoulakis, S., Mavrogianni, A., Jones, B., & Oikonomou, E. (2014). The modifying effect of the building envelope on population exposure to $PM_{2.5}$ from outdoor sources. Indoor Air, 24(6), 639– 651. https://doi.org/10.1111/ina.12116

Underhill, L. J., Fabian, M. P., Vermeer, K., Sandel, M., Adamkiewicz, G., Leibler, J. H., & Levy, J. I. (2018). Modeling the resiliency of energy-efficient retrofits in low-income multifamily housing. Indoor Air, 28(3), 459–468. https://doi.org/10.1111/ina.12446

Underhill, L. J., Dols, W. S., Lee, S. K., Fabian, M. P., & Levy, J. I. (2020). Quantifying the impact of housing interventions on indoor air quality and energy consumption using coupled simulation models. Journal of Exposure Science and Environmental Epidemiology, 30(3), 436–447. https://doi.org/10.1038/s41370-019-0197-3

Vardoulakis, S. (2009). Human exposure: Indoor and outdoor. In Air Quality in Urban Environments, ed. R. M. Harrison and R. E. Hester, The Royal Society of Chemistry, 2009, vol. 28, ch. 5, 85-107. https://doi.org/10.1039/9781847559654-00085.

Venkatesan, P. (2016). WHO report: air pollution is a major threat to health. The Lancet Respiratory Medicine, 4(5), P351. https://doi.org/https://doi.org/10.1016/S2213-2600(16)30014-5

Walton, G. N. (1989). AIRNET - A Computer Program for Building Airflow Network Modelling. National Institute of Standards and Technology 89-4072, April, 77.

Walton, G. N., & Dols, W. S. (2005). CONTAM 2.4 user guide and program documentation. National Institute of Standards and Technology, Gaithersburg, MD. https://doi.org/10.6028/NIST.IR.7251

Wang, L., & Chen, Q. (2007). Analysis on the well-mixing assumptions used in multizone airflow network models. IBPSA 2007 - International Building Performance Simulation Association 2007, 2001, 1485–1490.

WHO (2013). Health effects of particulate matter: policy implications for countries in eastern Europe, Caucasus and central Asia. World Health Organization. Regional Office for Europe. https://iris.who.int/handle/10665/344854

WHO (2021). WHO global air quality guidelines: Particulate matter ($PM_{2.5}$ and PM10), ozone, nitrogen dioxide, sulfur dioxide and carbon monoxide. Geneva: World Health Organization. https://doi.org/10.1016/j.envint.2021.106595

Yu, Y., Megri, A. C., & Jiang, S. (2019). A review of the development of airflow models used in building load calculation and energy simulation. Building Simulation, 12(3), 347–363. https://doi.org/10.1007/s12273-018-0494-0

Supplementary Table

Table S1: A summary of the input parameters of CONTAM(.prj) file and EnergyPlus (.idf) file

Category	Parameter	Symbol [unit]	Data Source	Attribution Level
Building/Zone Variants	Zone Height	H [m]	CAD Drawings (Architectural Plans, Sections and Elevations from HEI EFM)	Development of CONTAM Project Files [.prj] for each Higher Education Building that includes detailed zones geometries, adjacencies and juxtapositions.
	Zone Area	A [m^2]		
	Zone Volume	V [m^3]		
	Zone Orientation	φ [°]		
Building Construction Year	External Building Envelope Effective Leakage Area	ELA [cm^2/m^2]	NIST[1] Library	Calculation of Building Envelope Air Permeability Values Q_{50} [$m^3/h/m^2$] after performing CONTAM Pressurisation Test at ΔP=50 Pa
	Building Envelope and Building Components Thermal Transmittance Value	U-Value [W/m^2K]	CAD Drawings (Wall Sections and Material Specifications from HEI EFM)	Development of Building Age Representative Material and Construction .idf files to Perform Dynamic Thermal Simulation in EnergyPlus
Window Parameters	Window Glazing Area	A_{wl} [m^2]	CAD Drawings (Architectural Plans, Sections and Elevations from HEI EFM)	Calculate the amount of Heat Gain and Heat Loss in EnergyPlus
	Window Opening Area	A_{wo}[m^2]	EFM Heating Policy Plan	Window Opening Schedules to Account for Natural Ventilation in Cooling Season
	Window Leakage Area	A_{wl} [cm^2/m]	NIST[1] Library	Development of Window Leakage Elements in CONTAM Project Files using a Power Law Model $Q= C(\Delta P)^n$
Building User Characteristics	Maximum Occupancy	Occ_m	UK University Space Planning Guide for Space Standards and University Timetables for Different Space Types.	Space Use / Occupancy Schedules in CONTAM and EnergyPlus to Account for Indoor Heat Gains and CO_2 Generation Rates, and the Calculation of $PM_{2.5}$ Exposure Levels.
	Occupancy Density	Occ_d [m^2/person]		
	Occupancy Level	Occ	Assumed Occupancy Data was Used	
Pollutant Characteristics	$PM_{2.5}$ Deposition Rate	k [h^{-1}]	Literature	Identify Sink Elements in CONTAM Project Files to represent the loss of $PM_{2.5}$ in Indoors.
Airflow Characteristics	Flow Exponent	n	CONTAM User Guide	Indicator of the Nature of Airflow (Turbulent or Laminar), Typical Values for Infiltration Airflow between 60 and 70

	Flow Coefficient	C		Airflow Openings Dynamic Effects, Typical Values C=60 for Small Openings and slightly higher for Larger Openings
	Wind Pressure Coefficient	C_p	Swami and Chandra Model	Calculate Wind Pressure Coefficients for Different Wind Angles in CONTAM to account for Wind Pressure Effect on Building Façade
Ambient Weather Characteristics	Outdoor Temperature	T_{amb} [°C]	Local Weather Stations (Sheffield's Weston Park Weather Station)	Generating EnergyPlus Weather Files (.epw) and CONTAM Weather Files (.WTH) using Actual Meteorological Year (AMY) Data
	Wind Speed	v [m.s^{-1}]		
	Wind Direction	u [°]		
	Ambient $PM_{2.5}$ Concentrations	C_{amb} [μg/m^3]	Local Pollutant Monitoring Station (Sheffield Devonshire Green (UKA00575))	Generating CONTAM Ambient $PM_{2.5}$ Concentration Levels Files (.CTM) using Hourly Data
Indoor Environment Characteristics	Heating Season Indoor Air Temperature	T_{in} [°C]	University of Sheffield Indoor Space Heating Policy	Development of EnergyPlus Indoor Space Heating Schedules and Setpoints to Control Indoor Air Temperature for the Co-Simulation